An Hourly Assimilation–Forecast Cycle: The RUC

Stanley G. Benjamin, Dezsö Dévényi,[*] Stephen S. Weygandt, Kevin J. Brundage,[+] John M. Brown,
Georg A. Grell,[*] Dongsoo Kim,[*] Barry E. Schwartz, Tatiana G. Smirnova,[*]
and Tracy Lorraine Smith[+]

NOAA/Forecast Systems Laboratory, Boulder, Colorado

Geoffrey S. Manikin

NCEP/Environmental Modeling Center, Camp Springs, Maryland

ABSTRACT

The Rapid Update Cycle (RUC), an operational regional analysis–forecast system among the suite of models at the National Centers for Environmental Prediction (NCEP), is distinctive in two primary aspects: its hourly assimilation cycle and its use of a hybrid isentropic–sigma vertical coordinate. The use of a quasi-isentropic coordinate for the analysis increment allows the influence of observations to be adaptively shaped by the potential temperature structure around the observation, while the hourly update cycle allows for a very current analysis and short-range forecast. Herein, the RUC analysis framework in the hybrid coordinate is described, and some considerations for high-frequency cycling are discussed.

A 20-km 50-level hourly version of the RUC was implemented into operations at NCEP in April 2002. This followed an initial implementation with 60-km horizontal grid spacing and a 3-h cycle in 1994 and a major upgrade including 40-km horizontal grid spacing in 1998. Verification of forecasts from the latest 20-km version is presented using rawinsonde and surface observations. These verification statistics show that the hourly RUC assimilation cycle improves short-range forecasts (compared to longer-range forecasts valid at the same time) even down to the 1-h projection.

1. Introduction

Many hazardous weather events are difficult to forecast even with very short lead time. Specific examples include winter precipitation, convective storms, clear-air turbulence, icing, and low ceiling and visibility. Accurate short-term forecasts of these phenomena are clearly important for the protection of life and property and also have significant economic value. Potential applications include aviation (air traffic management, flight routing, and estimated fuel needs), agriculture, recreation, and power.

Many different observations have become available over the United States (and globally), with frequencies of an hour or less. These include commercial aircraft, wind profilers, geostationary satellites, radars, ground-based GPS, and automated surface reports. The availability of these observations facilitates high-frequency updating of short-range numerical forecasts, with the expectation that forecasts initialized with more recent observations will be more accurate.

The Rapid Update Cycle (RUC), an operational mesoscale data assimilation and numerical forecast system run at the National Centers for Environmental Prediction (NCEP), is designed to provide this type of frequently updated numerical forecast guidance. The RUC runs at the highest frequency of any forecast model at NCEP, assimilating recent observations to provide hourly updates of current conditions (analyses) and short-range numerical forecasts. The RUC is unique among operational numerical weather prediction (NWP) systems in two primary aspects: its hourly forward assimilation cycle and its use of a hybrid isentropic–terrain-following vertical coordinate for both its assimilation and forecast model components.

The first operational implementation of the Rapid Update Cycle (RUC1) occurred in 1994 (Benjamin et al. 1994), with a 3-h assimilation cycle (Benjamin et al.

* Additional affiliation: Cooperative Institute for Research in the Environmental Sciences, University of Colorado, Boulder, Colorado.

+ Additional affiliation: Cooperative Institute for Research in the Atmospheres, Colorado State University, Fort Collins, Colorado.

Corresponding author address: Stan Benjamin, NOAA/FSL, 325 Broadway, R/E/FS1, Boulder, CO 80305.
E-mail: stan.benjamin@noaa.gov

TABLE 1. A history of spatial resolution and assimilation frequency in implementations of the operational Rapid Update Cycle at NCEP.

Model/ assimilation system	Horizontal resolution	Number of vertical levels	Assimilation frequency	Implemented at NCEP
RUC1	60 km	25	3 h	Sep 1994
RUC2	40 km	40	1 h	Apr 1998
RUC20	20 km	50	1 h	Apr 2002

1991) in which a new analysis was produced every 3 h using the previous 3-h forecast as a background. Major upgrades (Table 1) were made in horizontal and vertical resolution in 1998 (RUC2) and 2002 (RUC20). The 2002 version (hereafter RUC) employs 20-km horizontal resolution, 50 vertical levels, and a 1-h assimilation cycle.

In this paper we describe the RUC cycle and assimilation methods, discuss issues relevant to high-frequency assimilation, and illustrate the RUC forecast improvement that occurs through the high-frequency assimilation of recent observations. A companion paper (Benjamin et al. 2004) describes the RUC forecast model in detail, with emphasis on the hybrid isentropic-sigma coordinate.

In section 2, the RUC 1-h cycle design is described, along with a discussion of two important issues for high-frequency intermittent assimilation: noise control via application of a digital filter and grouping of observations into time windows. Section 3 follows, with specific information on the current operational version of the RUC, including horizontal and vertical domain, the definition of the hybrid isentropic–sigma coordinate, and the types of observational data utilized. An overview of the RUC unified analysis framework is given in sec-

tion 4, along with implementation details for both the optimal interpolation (OI; operational in early 2003) and three-dimensional variational data assimilation (3DVAR; operational as of 27 May 2003) techniques. Section 4 also includes a discussion of the background error covariances in hybrid isentropic–sigma coordinates. In section 5, surface and upper-air verification results are presented for RUC forecast projections ranging from 1 to 24 h. Using these results, the ability of the RUC to improve short-term forecast skill through the use of hourly data assimilation is assessed. Conclusions and future plans for the Rapid Update Cycle are provided in section 6.

2. Design of the RUC 1-h assimilation–forecast cycle

The RUC uses a forward intermittent assimilation cycle, as depicted in Fig. 1. Every hour, recent observations are assimilated using the previous 1-h RUC model forecast as a background to produce a new estimate of 3D atmospheric fields. Specifically, the observation-minus-forecast residuals (*innovations*) are analyzed to produce an estimate of the 3D multivariate *forecast error field,* also called the *analysis increment.* This analysis increment is added to the 1-h forecast background to produce the new analysis. The 1-h forecast contributes information from previous observations into the current analysis through the filter of the forecast model. The observation types used by the RUC are discussed in section 3b and summarized in Table 2.

The design of a prototype RUC [known then as the Mesoscale Analysis and Prediction System (MAPS)] 3-h assimilation cycle based on a pure isentropic coordinate and 80-km horizontal resolution was described
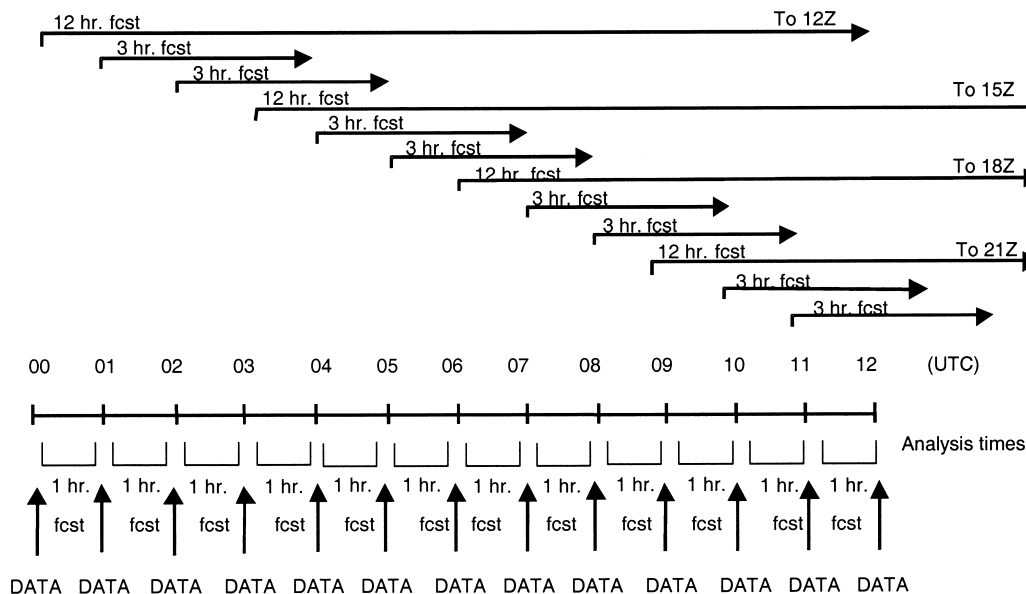

FIG. 1. Schematic of 1-h Rapid Update Cycle operational configuration at NCEP in early 2003.

TABLE 2. Observational data used in the RUC as of spring 2003.

Data type	~Number	Frequency
Rawinsonde (including special obs)	80	/12 h
NOAA 405-MHz profiler wind	31	/ 1 h
Boundary layer (915 MHz) profiler wind[d]	24	/ 1 h
RASS virtual temperatures[d]	10	/ 1 h
VAD winds (WSR-88Ds)[a]	110–130	/ 1 h
Aircraft (ACARS)[b] (wind, temperature)	1400–4500	/ 1 h
Surface/METAR—land (V, p_{sfc}, T, T_d)	1500–1700	/ 1 h
Surface/Mesonet—land[d]	2500–4000	/ 1 h
Buoy	100–150	/ 1 h
GOES precipitable water	1500–3000	/ 1 h
GOES cloud-drift winds	1000–2500	/ 1 h
GOES cloud-top pressure/temperature	~10 km resolution	/ 1 h
SSM/I[c] precipitable water	1000–4000	/ 6 h
GPS precipitable water[d]	200	/ 1 h
Ship reports	5–40	/ 3 h
Reconnaissance dropwinsonde	0–10	/variable

[a] Weather Surveillance Radar-1988 Doppler.
[b] Aircraft Communications, Addressing, and Reporting System.
[c] Special Sensor Microwave Imager.
[d] At FSL only as of Oct 2003.

by Benjamin et al. (1991). The first version of the RUC running at NCEP (from 1994 to 1998) also used a 3-h assimilation cycle, thus missing two-thirds of the hourly observations. Both of these 3-h cycles were continuous, in the sense that RUC forecasts were always used as the background for the next analysis. This internal cycling of regional models has become more common since that time, with the NCEP Eta Data Assimilation System (EDAS) changing to fully cycled atmospheric variables in 1998 (Rogers et al. 1999).

The RUC intermittent assimilation procedure falls within a class of schemes that include all sequential data assimilation methods (specifically including optimum interpolation, 3DVAR, and nudging schemes). As such, it can be interpreted in the general framework of Kalman filtering (Daley 1991, section 13.3). In the Kalman filtering approach [using the unified notation of Ide et al. (1997)], a forecast step ($\mathbf{M}$) is used to advance the model state ($\mathbf{x}$) from analysis ($\mathbf{x}^a$) or forecast ($\mathbf{x}^f$) and forecast error covariance ($\mathbf{P}^f$) in time:

$$\mathbf{x}^f(t_i) = \mathbf{M}_{i-1}[\mathbf{x}^a(t_{i-1})], \tag{1}$$

$$\mathbf{P}^f(t_i) = \mathbf{M}_{i-1}\mathbf{P}^a(t_{i-1})\mathbf{M}_{i-1}^T + \mathbf{Q}(t_{i-1}), \tag{2}$$

where $\mathbf{Q}$ is the model error covariance. This is followed by an analysis step to update the model state and analysis error covariance ($\mathbf{P}^a$):

$$\mathbf{x}^a(t_i) = \mathbf{x}^f(t_i) + \mathbf{K}_i\mathbf{d}_i, \tag{3}$$

$$\mathbf{P}^a(t_i) = (\mathbf{I} - \mathbf{K}_i\mathbf{H}_i)\mathbf{P}^f(t_i), \tag{4}$$

where

$$\mathbf{d}_i = \mathbf{y}_i^o - \mathbf{H}_i[\mathbf{x}^f(t_i)] \tag{5}$$

is the innovation vector, $\mathbf{y}$ is the observation vector, $\mathbf{H}$ is the forward transformation from the model to the observation (including interpolation and variable transformation), and

$$\mathbf{K}_i = \mathbf{P}^f(t_i)\mathbf{H}_i^T[\mathbf{H}_i\mathbf{P}^f(t_i)\mathbf{H}_i^T + \mathbf{R}_i]^{-1} \tag{6}$$

is the Kalman gain, and $\mathbf{R}$ is the observation error covariance matrix.

Because Kalman filtering in its original formulation is not practical for application in present numerical forecasting systems, some simplification is necessary to develop realizable data assimilation systems. As noted by Bennett (1992, p. 83) and elaborated in detail in Robinson et al. (1998), the nudging method can be considered as a special simplified Kalman filter with a gain matrix $\mathbf{K}$ that is diagonal and constant in time. Similarly, optimum interpolation/3DVAR-based intermittent assimilation, as applied in the RUC, is another special case of the Kalman filter with empirically deduced forecast error covariance matrices (Robinson et al. 1998). In the RUC assimilation cycle, the forecast error covariances are not advanced forward in time, but are used in an adaptive manner resulting from the adaptive hybrid isentropic–coordinate formulation [see section 4 in this paper; also, Benjamin (1989)]. A similar approach, which does not use the adaptive model coordinate system but makes use of the background potential temperature field, was proposed in Daley and Barker (2001) and in Riishojgaard [1998, his Eq. (16)] to introduce anisotropic correlation structures.

Two key issues associated with high-frequency forward assimilation are now discussed: control of noise in the very short-range (1 h) forecasts used as the background for subsequent analyses and time window design for grouping observations assumed to be valid at the analysis time.

a. Noise control for background forecast

Without proper control of spurious gravity waves during the initial forecast hour, an intermittent hourly assimilation cycle will accumulate noise and imbalance, resulting in poorer performance than that from a less frequent assimilation cycle. Imbalances in the analyzed fields can be removed through initialization procedures, but the resultant changes to mass and wind may be significant compared to the analysis increment. This poses a particular challenge for high-frequency mesoscale assimilation systems such as the RUC, in that mesoscale balance in the analysis increment is difficult to achieve, yet the 1-h forecasts must appropriately match observations valid 1 h later.

This challenge is overcome in the RUC through use of an adiabatic digital filter initialization (DFI; Lynch and Huang 1992) with an optimal filter (Huang and Lynch 1993). This initialization is well suited to the RUC model, for which it is difficult to diagnose normal modes because of the hybrid isentropic-sigma coordinate. In the RUC model, before each forecast, forward and backward adiabatic integrations of about 35 min are performed. Using the optimal digital filter, a weighted mean of the dynamic variables over the forward/backward integrations is then introduced as the actual initial condition for those variables. There is no filtering of moisture fields at this time. To monitor the effects of the DFI on the RUC model, the mean absolute surface pressure tendency (N_1 in Huang and Lynch 1993) is calculated as

$$N_1 = \overline{\left| \frac{\Delta p_{\text{sfc}}}{\Delta t} \right|}^{x,y} . \tag{7}$$

Figure 2 shows the N_1 parameter for a set of 6-h RUC model forecasts initialized with and without the DFI. At the first forward model time step (following the initialization, if performed), the N_1 parameter is reduced from 8.7 to 3.1 hPa h^{-1} with DFI for an OI analysis and from 5.1 to 2.7 hPa h^{-1} for a 3DVAR analysis (both analyses using the same background field and observational data). The model noise is also substantially reduced at the 1-h output time [5.2(3.4) to 1.6(1.4) hPa h^{-1} for OI (3DVAR) results]. These results are consistent with those shown for the European High Resolution Limited Area Model (HIRLAM) system (Fig. 18 of Gustafsson et al. 2001). This rapid (less than 1 h) reduction in gravity wave activity helps reduce aliasing in subsequent hourly analyses. Of course, these noise values are also a measure of the multivariate balance in the RUC analysis (discussed further in section 4) and the degree of numerical diffusion in the RUC model [very small, as described in Benjamin et al. (2004)].

b. Observation time windows

Aircraft observations are an especially important high-frequency data source for the RUC assimilation
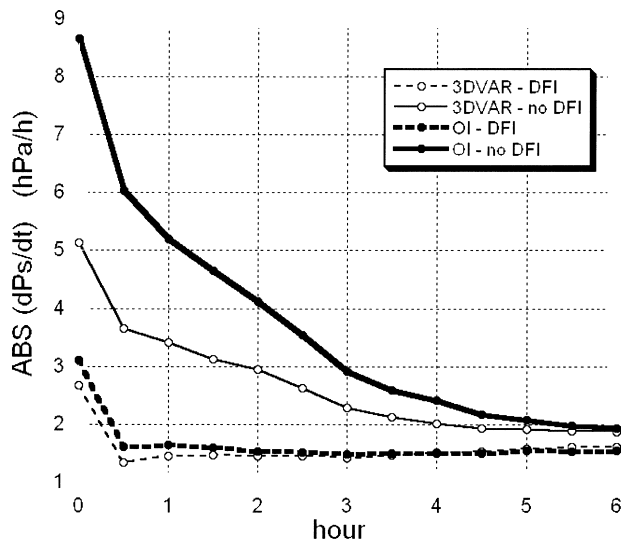

FIG. 2. Noise parameter over a single time step (30 s) in the RUC model with 3DVAR or OI analysis, both with and without application of DFI. For the case with initial conditions at 1200 UTC 19 Nov 2002, data points taken every 30 min of integration.

cycle; however, their distribution in space and time is irregular and dependent on the route structure of the commercial air carriers. The effective horizontal resolution of the aircraft observations can be varied by changing the duration of the time window within which they are grouped, but there is a trade-off between the spatial and temporal resolution. Aliasing is unavoidable with any discrete observational network in that small-scale waves will often be misrepresented as large-scale waves (Daley 1991, section 3d). The RUC is certainly vulnerable to problems with aliasing because of its reliance on aircraft data and the 1-h time windows currently assumed in its assimilation cycle. Thus, some attention is given in this section to the effects of time windowing on aliasing. These issues are discussed below in terms of aircraft data, but are equally valid for other observations of opportunity, such as ship data, and even the effects of ascent/descent times for rawinsonde/dropwinsonde soundings.

A temporal error is introduced in the assimilation if an observation is assumed to be valid at an analysis time that is not equal to the original observation time. This error can be reduced by using the first guess at the appropriate time (FGAT; e.g., Huang et al. 2002) to obtain a correct innovation. However, another component of this temporal error remains, the grouping of asynoptic innovations as if they were valid at the same time. Four-dimensional variational data assimilation (4DVAR) schemes avoid both portions of this temporal error by simultaneously fitting each observation along the model trajectory with time-appropriate fields (Rabier et al. 2000).

In the past, the combined temporal error has been commonly accepted in the intermittent data assimilation

systems utilized by many operational centers. In these schemes, observations are grouped within a time window several hours wide centered around an analysis time (e.g., Lorenc et al. 2000). A similar error occurs for assimilation schemes in which model forecasts are nudged toward observations (e.g., Stauffer and Seaman 1990, 1994; Leidner et al. 2001; Lorenc et al. 1991). Observations are assumed to be valid throughout the nudging time window, which is typically a few hours wide. The time validity problem becomes more significant as the resolution of the assimilation system is increased.

1) THE TRADE-OFF BETWEEN SPATIAL AND TEMPORAL RESOLUTION

A first-order solution to the time validity problem with aircraft data is to decrease the length of time windows for either intermittent or nudging data assimilation. For intermittent data assimilation, this also implies more rapid cycling and more frequent analyses. If the time window is decreased, the average time difference between the analysis time and observation time will also be decreased, which is clearly advantageous. Unfortunately, this also leads to a decrease in the volume of data valid within the time window. As Daley (1991, p. 85) states, "the local data density is time dependent" in the actual global observing system. Since the purpose of using observations within data assimilation is to correct background forecast error, the observation density must be sufficient to resolve that error on the scales for which a valid analysis is required. This effect is discussed briefly in the conclusion section of Macpherson (1991).

The analysis of a propagating feature in the forecast error field will suffer some kind of spatial distortion (stretching, compression, other) from the true pattern if defined with time-windowed asynoptic observations within that feature. Consider a simple case in which the observations are taken sequentially in the direction of the error pattern translation. For a slow-moving (10 m s^{-1}) error pattern, a 3-h window of observations within the error pattern can result in an apparent stretching of 100 km, even assuming steady-state propagation of the error feature. For a faster-moving (30 m s^{-1}) feature, for instance, one associated with a jet streak, a 100-km stretching error can result with only a 1-h time window. The observation density, analysis grid resolution, and scale and propagation speed of features to be resolved in an analysis all limit the size of the observation time window at its lower end. All of these same factors will also influence the nature of the distortion of the feature in the analysis increment.

This trade-off between spatial and temporal resolution for a given aircraft data time window is depicted in Fig. 3. In this example, the target phenomenon for this one-dimensional analysis is assumed to be a jet streak with a 480-km wavelength (λ), requiring an observation
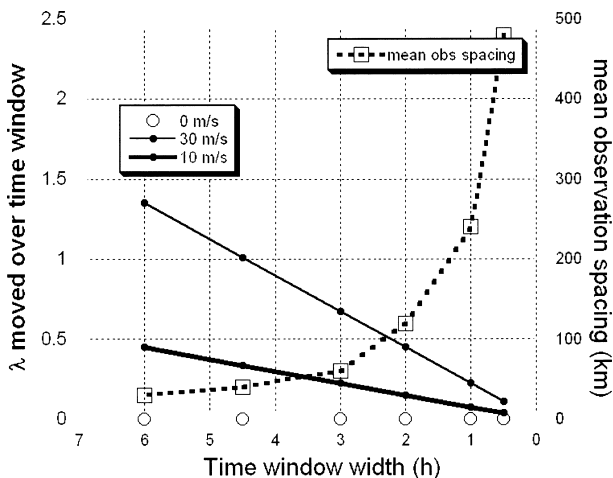

FIG. 3. Time window width as a function of two parameters for hypothetical time–space (1D) distribution of aircraft reports as described in section 2b(1). Solid lines and open circles show the fraction of jet streak wavelength λ (assumed as 480 km) moved over time windows of different duration for propagation speeds of 0, 10, and 30 m s^{-1} (corresponding to vertical axis on left). Dotted line shows mean observation spacing from this hypothetical distribution of aircraft reports evenly distributed in time as a function of time window width (corresponding to the vertical axis on right).

spacing of 30 km to resolve the feature with 16 data points. It is also assumed that a 6-h window of aircraft data (evenly distributed in time and space, not like the actual distribution of reports from a single aircraft) provides enough reports to resolve this feature with 30-km resolution. The trade-off between spatial and temporal resolution is critically dependent on the phase speed of the feature. If the jet streak is stationary, one can set the time window at infinity to obtain infinitely high horizontal resolution. If the jet streak is moving at the modest speed of 10 m s^{-1}, it has propagated 22% of its own wavelength in a 3-h window and 45% in a 6-h window, a substantial stretching deformity error. For a rapidly moving (30 m s^{-1}) mesoalpha-scale jet streak, even the 3-h window allows the feature to move 67% of its own wavelength. This error is demonstrated within the U.K. Met Office (UKMO) repeated insertion (nudging) assimilation system (not in operational use since October 1999) by Barwell and Lorenc (1985, their Fig. 5a and discussion on p. 116) for a specific case and by Macpherson (1991, his Fig. 8) for a mean analysis. The 1-h and 30-min windows greatly reduce the distortion, but the mean observation spacing is also considerably reduced (Fig. 3). This illustrates that if observations distributed through time, such as aircraft data, are broken into windows that are too small, they will be assimilated less effectively. This effect is described in greater detail in the next section.

2) A DEMONSTRATION OF THE CUMULATIVE EFFECT OF NARROW ANALYSIS TIME WINDOWING

Consider a case if aircraft data were the only data available. If the analysis time window is defined too
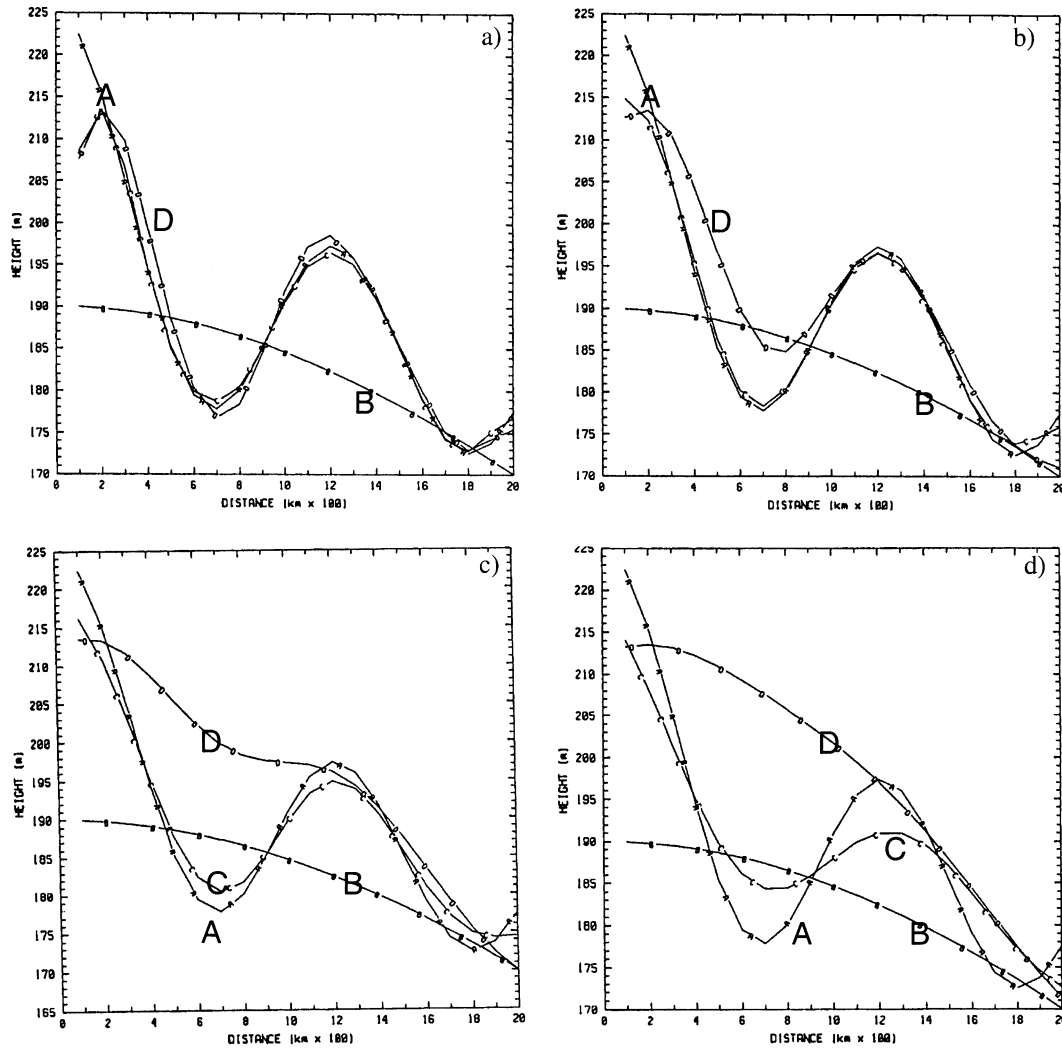
FIG. 4. One-dimensional analysis experiment results. Observations are specified at even-numbered grid points from the true field (curve A); no observational error perturbations are added. Differences from the background field (curve B) are analyzed to give a final analysis in two different ways: all 10 observations are used simultaneously in an OI analysis (curve C), and 10 successive analyses are made with 1 observation each (curve D). Gaussian scale for background error correlation model is (a) 200, (b) 400, (c) 600, and (d) 800 km.

narrowly, the volume of aircraft data would be so small that the analysis increments (corrections to forecasts) could resolve the true forecast error on only the largest scales. A simple experiment demonstrates this effect. An intermittent analysis–forecast cycle may be written as

$$\mathbf{x}^a(t) = \mathbf{A}(t)\mathbf{M}(\alpha)\mathbf{A}(t - \alpha)\mathbf{M}(\alpha)\mathbf{A}(t - 2\alpha) \cdots$$
$$\mathbf{M}(\alpha)\mathbf{A}(t - n\alpha), \qquad (8)$$

where the analysis steps $\mathbf{A}$ alternate with model forecasts $\mathbf{M}$, each of duration α hours to produce the analysis state $\mathbf{x}$ at time t. If the frequency of assimilation is increased and time windows are not allowed to overlap, the amount of data in each time window must decrease.

Consider the extreme case in which each time window contains only one observation and in which no forecast

steps are interleaved in a sequence of β successive analyses. This procedure may be written

$$x^a(t) = \mathbf{A}(1)\,\mathbf{A}(2) \cdots \mathbf{A}(\beta), \qquad (9)$$

where β is the total number of observations and number of time windows. This experiment is different from the iterative analysis procedure described by Bratseth (1986), since here different observations are used in each iteration.

The results of this successive analysis procedure [Eq. (9)] are compared with a typical analysis in which all of the β observations are used simultaneously (Fig. 4). In this one-dimensional analysis experiment, 10 observations were used with a univariate OI analysis. The observation error variance was assumed to be 0.08 times the background error variance, observation errors are
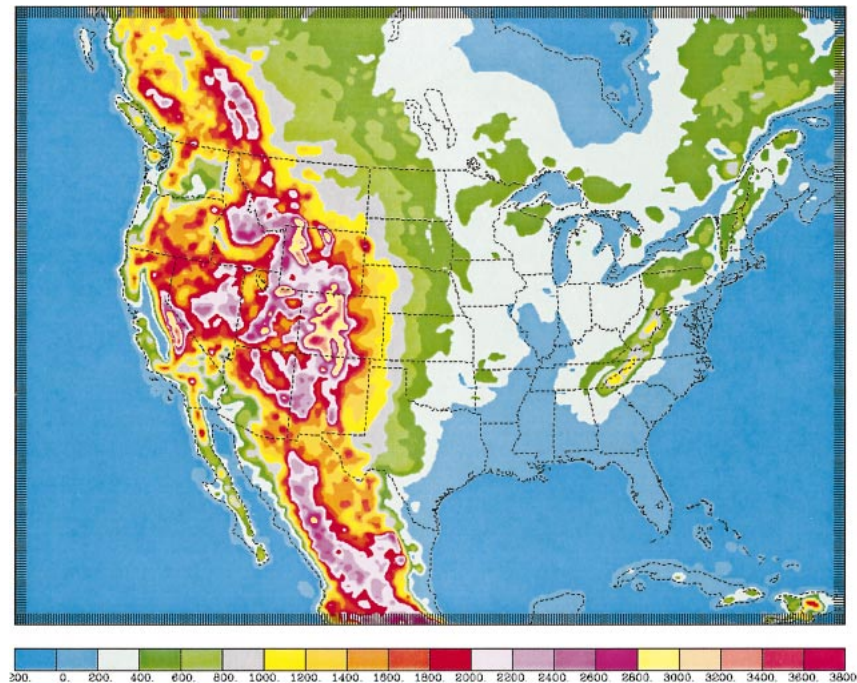
FIG. 5. Domain and terrain elevation of the 20-km version of the RUC. Contour elevation is 200 m. Grid dimensions are 301 by 225 points.

assumed to be uncorrelated, and a Gaussian function was used to describe the background error correlation. These parameters were left unchanged for all experiments, except that the scale coefficient in the background error correlation model was changed to show the effect of scale on the two experiments. The order of the observations was random in the successive analysis experiment.

If the assumed spatial correlation of background error is narrow (Fig. 4a), then there is little difference between the analysis with 10 observations (curve C) and the result of 10 successive analyses with one observation each (curve D). However, as the scale of the correlation model becomes larger (Figs. 4b–d), the successive analysis experiment (curve D) is increasingly unable to reproduce the correct field. Two beneficial characteristics of the analysis with all data are lost in the successive analysis experiment: the smaller scales in the background error cannot be resolved, and the interobservation correlations are not accounted for. These correlations are ordinarily accounted for in OI or variational analysis, but the successive analysis technique forces each observation to be considered as statistically independent of the others. In high-frequency data assimilation with narrow time windows, a model integration period will occur between each analysis step, and one may expect further problems from model noise generated by each analysis increment. In the example shown above, the trade-off between temporal and spatial resolution depends on the rate of change (phase speed, rotation, growth/dissipation, etc.) of the feature itself.

For an analysis/forecast cycle, the trade-off also depends on the rate of change of the forecast error pattern.

The problem described here concerning narrow time windowing is relevant to nudging as well as intermittent assimilation systems: if aircraft data are not allowed to sufficiently overlap during the nudging period to give adequate resolution of forecast error, then poorer results may be expected. Thus, the 1-h cycle used in the RUC makes it less vulnerable to the time validity problem but more vulnerable to spatial aliasing.

3. Operational configuration for the 20-km version of the RUC analysis

In the NCEP operational version as of early 2003, the RUC horizontal domain covers the contiguous 48 United States and adjacent areas of Canada, Mexico, and the Pacific and Atlantic Oceans with a 20-km grid (Fig. 5). A Lambert conformal projection with a 301 by 225 rectangular gridpoint mesh is used. The grid length is 20.317 km at 35°N. Because of the varying map-scale factor from the projection, the actual grid length in the 20-km RUC decreases to as small as 16 km at the northern boundary.

The surface elevation of the RUC is defined using a *slope envelope* topography (also shown in Fig. 5). The standard envelope topography is defined by adding the subgrid-scale terrain standard deviation (calculated from a 10-km terrain field) to the mean value over the grid box. By contrast, in the slope envelope topography, the terrain standard deviation is calculated with respect to

a plane fit to the high-resolution topography within each grid box. This gives more accurate terrain values, especially in sloping areas at the edge of high-terrain regions. It also avoids a tendency of the standard envelope topography to project the edge of plateaus too far laterally onto lower-terrain regions.

a. The RUC vertical coordinate

The RUC uses a generalized vertical coordinate configured as a hybrid isentropic–sigma coordinate in both the analysis and model. This coordinate is advantageous in providing sharper resolution near fronts and the tropopause (e.g., Shapiro 1981; Benjamin 1989). Johnson et al. (1993, 2000) have shown improved moisture transport and reduced vertical diffusion in a global model using a hybrid isentropic–sigma coordinate. In the RUC hybrid coordinate introduced by Bleck and Benjamin (1993), the pressure at each level is chosen either as that corresponding to a predefined virtual potential temperature (θ_v) value (an *isentropic* definition) or that corresponding to a minimum pressure spacing, starting upward from the surface (a *terrain-following* definition). The pressure at each level is chosen as the smaller of the two values. The RUC hybrid coordinate is discussed in much greater detail, including a table of reference θ_v values, in Benjamin et al. (2004).

In the RUC analysis, the spatial influence of observations [3D structure of forecast error covariances; $\mathbf{P}_f$ in Eq. (2)] is largely defined in isentropic space, leading to improved representation of airmass coherence and frontal structure. However, the analysis is still performed in a generalized vertical coordinate framework and is applicable to other coordinate systems. These characteristics are discussed in more detail in section 4.

The 20-km version of the RUC (Table 1) uses 50 vertical levels, with a reference θ_v value assigned to each level ranging from 224 to 500 K. The reference potential temperature spacing is 2 K between 294 and 322 K and 2–3 K from 270 to 355 K. This specification allows a relatively fine θ resolution through much of the troposphere and lower stratosphere. The terrain-following pressure spacing is 2.5 hPa in the first layer and maximizes at 15 hPa by the fifth layer above the surface.

A sample cross section of RUC native levels is displayed in Fig. 6. The cross section traverses the United States, passing south of San Francisco, California, through the eastern slopes of the Rocky Mountains in Colorado (where a mountain wave is evident between 300 and 600 hPa) and through southern Virginia on the East Coast. The cross section is for an RUC analysis valid at 1800 UTC 14 January 2002. The typical higher resolution near fronts and the tropopause using the RUC coordinate is apparent in this figure. Nonisentropic coordinates do not resolve these features as well. Also, the tendency for more terrain-following levels in warmer regions is evident (over the Pacific Ocean on the left-hand side of the figure, in this case). A classic cold
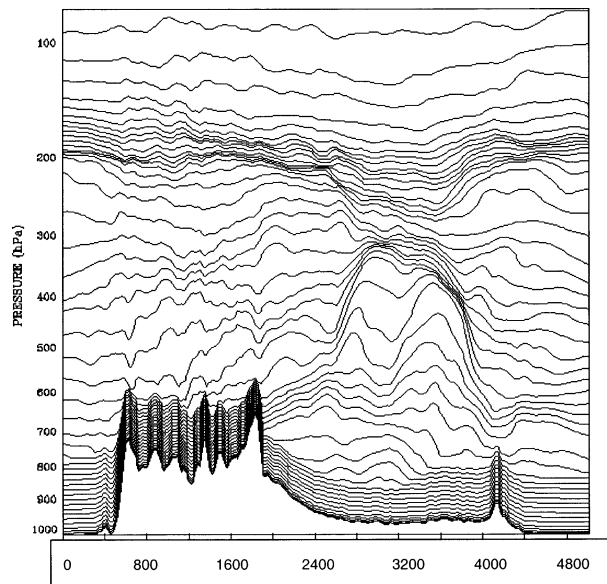

FIG. 6. Vertical cross section of RUC hybrid isentropic–sigma coordinate levels for 1800 UTC 14 Jan 2002. The cross section is oriented approximately west–east through California on the left-hand side, Colorado, and the Appalachian Mountains.

dome is evident over the central United States, with a lowered tropopause and frontal zones extending to the surface on both sides. Generalized analysis/model levels that are isentropic in one part of the domain can become terrain following in other parts of the domain.

b. Observational data assimilated in the RUC and calculation of innovations

In order for a high-frequency assimilation cycle to result in improved short-range forecasts, adequate high-frequency observations must exist over the domain of the analysis and forecast model. Over the last 10 years, the volume of observational data over the United States has increased, along with the sophistication of techniques to assimilate those observations.

A summary of observational data available to the RUC as of spring 2003 is shown in Table 2. A large variety of observation types are assimilated, although many of them are limited in horizontal or vertical spatial coverage. The longest-standing atmospheric observing systems, rawinsondes, and surface weather observations are the only ones that provide complete observations of wind, pressure, temperature, and moisture. High-frequency wind observations above the surface are available from commercial aircraft (e.g., Moninger et al. 2003), wind profilers, satellite-estimated cloud motion, and radars [velocity–azimuth display (VAD)]. High-frequency temperature observations above the surface assimilated by the RUC include commercial aircraft and a few from the Radio Acoustic Sounding System (RASS). High-frequency moisture observations above the surface used in the RUC analysis are precipitable

water retrievals from satellites [Geostationary Observational Environmental Satellite (GOES) and polar orbiter] and from ground-based GPS (Wolfe and Gutman 2000; Gutman and Benjamin 2001) and GOES cloud-top pressure/temperature retrievals (Schreiner et al. 2001). The "cutoff" time for availability of observations is very short with the RUC, generally about 20 min after the analysis valid time, except at 0000 and 1200 UTC when it is extended to 50 min to allow receipt of rawinsonde data.

Most of the observations that are not subject to time windowing (section 2b) are actually valid 15–30 min before their labeled time. For instance, rawinsondes are launched about 45 min before valid time, surface observations are taken 15 min before valid time, and wind profiler hourly observations are hourly means centered 30 min before valid time. Accordingly, the time window used in the RUC for aircraft and cloud-drift wind observations is a 1-h window centered 30 min before "valid" time. This 15–30-min offset between labeled and actual valid time is present not only in the RUC but in other operational systems initialized with the same observations. If a subhourly FGAT was used (as suggested from results regarding 1-h persistence forecasts shown in section 5a), this offset between labeled and actual valid time for RUC grids should be accounted for.

The accuracy of an analysis is dependent on the effectiveness of algorithms used to match observations with the background values ("forward transformations," **H**, in section 2) for calculation of observation-minus-background innovations. These forward models from the background to the observation may include variable transformations. For near-surface observations, they should also account for elevation differences between the background and observations using expected boundary layer structure. For surface observations, this treatment in the RUC analysis uses surface layer similarity to match 2-m temperature and moisture observations and 10-m winds to the RUC background whose lowest levels is at 5 m above the surface. Surface observations including a station pressure (from an altimeter setting) and station elevation are reduced to a surface pressure at the model elevation and then to a height innovation at the model surface pressure to be used in the multivariate z/u/v analysis described in the next section. Observations of pressure reduced to sea level are not used in the RUC, since altimeter setting is less ambiguous and more commonly available over North America. Rawinsonde profiles from mandatory and significant level data are further interpolated to each model level, yielding additional data points. This forces the analysis to fit the near-linear structures implied by the absence of intermediate significant levels. The processing of each observation type to provide the best match between the observation and background is discussed in detail by Devenyi and Benjamin (2003).

c. Lateral boundary conditions

For any limited-area model, the skill is increasingly controlled by the lateral boundary conditions (LBC) as the duration of a forecast increases. The LBCs for the RUC model, both in operations at NCEP and runs at the Forecast Systems Laboratory (FSL), are relaxed (Davies and Turner 1977) toward the NCEP Eta Model (Black 1994; currently initialized every 6 h), linearly interpolated between 3-h output times. For RUC forecasts initialized at 0000 or 1200 UTC, the Eta Model run used for LBCs is always that initialized 6 h earlier (e.g., the 0600 UTC Eta run is used to prescribe LBCs for the RUC run initialized at 1200 UTC). This choice is made to provide RUC guidance to users as soon as possible as opposed to running the RUC model after the current Eta run is available. From a forecast skill standpoint, a 24-h RUC forecast run in this real-time configuration is controlled, to some extent, by the skill of the 30-h Eta forecast. Similarly, 12-h RUC forecasts are driven toward the information of the 18-h Eta forecasts valid at the same time. RUC forecasts can also be run using LBCs from Eta Model runs initialized at the same time to provide a model intercomparison, but that was not done for the results shown here. LBCs for the RUC can be prescribed from other models of course, such as the NCEP Global Forecast System (GFS) model, but the Eta Model has been used for the RUC in operational runs up to this point since it is available sooner and has a higher horizontal resolution than the GFS model.

4. Unified analysis framework in a generalized vertical coordinate

A unified framework for the RUC analysis has been developed that is general in two regards: it uses the vertical coordinate of the background model (hybrid isentropic–sigma for the RUC but applicable to other coordinates as well), and it can use solvers from either OI or 3DVAR techniques. The analysis framework includes ingest and preprocessing of the observations described in section 3, and the calculation of innovations [discussed briefly in section 3 and in more detail by Devenyi and Benjamin (2003)]. The background field is usually the previous 1-h RUC forecast (Fig. 1) in its native coordinate. Quality control is applied for observations, using the techniques described later in section 4e. The same data structure is used for observations, innovations, and metadata (location, observation type, etc.) rather than using different arrays for each observation type, allowing new observation types to be added without necessarily requiring new arrays. Observation and background errors are specified in the generalized framework.

The background error spatial covariances in the RUC analysis are defined in a quasi-isentropic space. Thus, the influence of observations in correcting a background is adaptive depending on the 3D thermal structure in

TABLE 3. RUC native coordinate variables and modification in the RUC analysis; MV refers to multivariate mass/wind analysis and UV to univariate analyses.

	Variables in native RUC analysis	Updating from observations in RUC analysis
p	Pressure	MV analysis from z increment, hybrid adjust
θ_v	Virtual potential temperature	MV analysis, UV θ_v analysis
u, v	Horizontal wind components	MV analysis
q_v	Water vapor mixing ratio	Moisture analysis outer loop
q^*	Hydrometeor mixing ratios (cloud water, ice, rainwater, snow, graupel) and ice particle number concentration	Cloud analysis with GOES cloud-top data
	Land surface variables	
—	Soil temperature, snow temperature—top level	From MV and UV θ_v analysis increment at lowest atmospheric level
—	Soil moisture	Not modified
—	Snow water equivalent	Not modified
(z calculated hydrostatically, all p/z obs converted to z innovations at a given pressure)		

the vicinity of the observations. The background error correlations in the RUC OI for all variables are specified as separable vertical and horizontal correlations between points m and n:

$$C_{i,j}^{m,n} = C_h(r_{i,j})C_v(|\theta_m - \theta_n|), \qquad (10)$$

where C_h and C_v are the horizontal and vertical correlations, r is the horizontal distance, and θ is virtual potential temperature [see similar equation in Riishojgaard (1998)]. The RUC 3DVAR effectively uses the same covariance structure shown in Eq. (10) in levels resolved as isentropic levels but not in those resolved as terrain-following levels (Devenyi and Benjamin 2003).

The hypothesis of horizontal and vertical separability of background error covariances is less problematic with the RUC quasi-isentropic coordinate system than in quasi-horizontal coordinate systems. Much of the vertical covariance variation is projected onto insentropic levels with the RUC coordinate, analogous to the projection of vertical motion onto horizontal motion on sloping isentropic surfaces in isentropic forecast models (see Benjamin et al. 2004 for further discussion). Also, with the RUC hybrid vertical coordinate system, the aspect ratio (ratio of vertical and horizontal scales) approaches zero for a completely adiabatic atmosphere. Benjamin (1989) demonstrates the effects of the assumption that the forecast error correlation structure is more horizontally isotropic in the isentropic system than in height- or pressure-based systems.

A multivariate mass/wind analysis with a balance constraint using all wind and height innovations (including those calculated from surface pressure observations at a given elevation) is carried out to obtain a wind analysis increment field. The associated height analysis increment (z') is vertically differentiated to obtain a virtual temperature increment. This temperature increment is added to the background θ_v (virtual potential temperature) field, yielding an updated field that reflects the multivariate analysis. A univariate θ_v analysis is then applied in which in situ temperature observations are assimilated (using background water vapor mixing ratio if not available from the observation). A surface pressure increment is also calculated from the height increment at the lowest level from the multivariate analysis step.

Next, the moisture field is analyzed univariately (using the logarithm of the water vapor mixing ratio as the analysis variable). Two other moisture analysis procedures are also carried out: first, the assimilation of GOES cloud-top pressure [Benjamin et al. (2002b); described further in section 4d] and, second, the assimilation of integrated precipitable water (IPW) observations, using an OI-based columnar adjustment (Smith et al. 2000). These three procedures are performed sequentially within each of two iterations of an outer moisture analysis loop in which the moisture background and innovations are updated after each procedure is applied. In this manner, a mutual adjustment between these different observation types is forced.

A summary of fields updated in the RUC analysis is presented in Table 3. Note that the upper level of soil or snow temperature is also updated from surface air temperature analysis increments to preserve the air surface temperature difference from the background field. [In general, the regional evolution of soil temperature and moisture fields and snow water equivalent and snowpack temperature fields has been found to give satisfactory results in the RUC (Smirnova et al. 1997, 2000; Benjamin et al. 2004).] These fields are strongly dependent on the accuracy of the series of 1-h forecasts produced by the RUC and, therefore, vulnerable to precipitation spinup (or spindown) problems. (Verification of RUC precipitation forecasts over a 24-h period aggregated from a series of eight 3-h forecasts shows nearly equal accuracy to those summed from two 12-h forecasts; results not shown.) Hydrometeor fields are also cycled and modified using the cloud analysis technique described in section 4d, contributing to this result. Current development efforts to add radar reflectivity to this hydrometeor analysis (Kim et al. 2002) should further

improve the RUC 1-h precipitation forecasts. The land surface model and mixed-phase cloud microphysics used in the RUC model are both described in more detail in the companion paper by Benjamin et al. (2004).

Mapping of observations and background values to vertical levels is carried out using the 3D pressure of the background field, without regard to the algorithm defining the vertical coordinate that resulted in the 3D pressure field. As a final processing step (which is specific to the hybrid coordinate used in the RUC model), a vertical regridding (interpolation) occurs for all variables that restores them to the RUC hybrid isentropic-sigma coordinate definition described in Benjamin et al. (2004). (This is approximately a 10-line code section that can be replaced by another vertical coordinate definition, if necessary, such as a pure sigma-pressure definition.)

Postprocessing of native RUC analysis fields is then performed to diagnose many other variables, including height (via hydrostatic integration), special level variables (freezing, maximum wind, and tropopause), cloud top, ceiling, visibility, convection-related indices, potential wind gust, and boundary layer height (Benjamin et al. 2002a). Hourly time series of full output at selected stations are created as part of the RUC postprocessing.

a. Three-dimensional optimum interpolation analysis

The optimal interpolation multivariate analysis used in the RUC follows the unified analysis framework described above, but with the following additions.

Observations are subjected to a superobservation processing (Lorenc 1981) to prevent the use of pairs of observations that are sufficiently close together to result in an ill-conditioned observation–observation covariance matrix (Benjamin 1989). Search tables are built to allow a quick identification of all observations within each grid volume. A ''volume method'' is used by which a limited set of observations is used to influence a set of grid points, to reduce the number of matrix computations (Lorenc 1981). The search strategy to identify observations (and residuals) to be used for each set of grid points includes use of eight directional sectors and a search for observations within a limited number of vertical layers from the grid points for which an analysis increment is to be computed. For generalized vertical coordinate levels that happen to be isentropic, this observation selection will tend to occur along isentropic surfaces. Up to 56 observations are chosen for the mass/wind analysis in each analysis volume, and up to 16 observations for univariate analyses. These limits confine the number of matrix inversion calculations and, therefore, the computational requirement for the analysis. The multivariate mass/wind analysis uses a geostrophic coupling coefficient of 0.5, except near the surface, where this coefficient is reduced to as low as 0.3.

Horizontal correlations of background error are described using coefficients of a second-order autoregressive (SOAR) function. Vertical correlations of background error in the RUC OI analysis are described explicitly as a function of potential temperature separation (Benjamin 1989), as shown in Eq. (10) above. As with any OI scheme in which limited numbers of observations are used for separate analysis volumes for which solutions are made of the analysis increment, the prescribed correlation models are truncated at the distances at which observations are found.

The effect of the truncated background error covariance model in the OI solutions with separate analysis volumes is depicted in Fig. 7a, a vertical west–east cross section of the u wind component analysis increment for a case from May 2002. Discontinuities from this truncation are apparent in both the horizontal and vertical dimensions in Fig. 7a, in contrast with the continuous analysis increment field produced by a 3DVAR analysis (Fig. 7b) for the same case and observational data. The effects of the small-scale noise produced by the truncated background error covariance in the OI solution are also evident in the mean surface pressure tendencies in subsequent forecasts shown in Fig. 2. The reduced noise at initial time steps and 1-h forecast times from the 3DVAR analysis, even after application of a digital filter initialization (section 2a) are related to these differences in the spectra at short wavelengths between analyses using the 3DVAR (fully 3D) and OI (with limited observations influencing different analysis volumes) techniques. Gustafsson et al. (2001) also showed a similar reduction in short-range forecast noise in replacing OI with a 3DVAR analysis and also attributed this behavior to the use of limited observations in OI (truncated covariances) versus global use of data in 3DVAR.

b. Three-dimensional variational analysis

The design of the 3DVAR version of the RUC analysis closely follows that applied in OI (see section above). A detailed description of RUC 3DVAR is given in Devenyi and Benjamin (2003); here we summarize only its basic features. In the RUC 3DVAR, the standard form of incremental cost function is minimized. The control variables are streamfunction (ψ) and velocity potential (χ) (both scaled by grid distance), unbalanced height, virtual potential temperature, and the natural logarithm of water vapor mixing ratio.

The analysis is performed on a 56-level modification of the 50 native RUC hybrid sigma–isentropic model levels. The isentropic projection for the RUC 3DVAR is accomplished through mapping observations (and innovations) to k space (56 levels) using the 3D pressure of the hybrid isentropic–sigma background 1-h RUC forecast. Thus, the isentropic projection is present in the RUC 3DVAR only in regions of the 3D background resolved as isentropic levels (typically upward from 150 to 300 hPa above the surface). The actual variational solution is fully generalized in 3D (i, j, k) space and
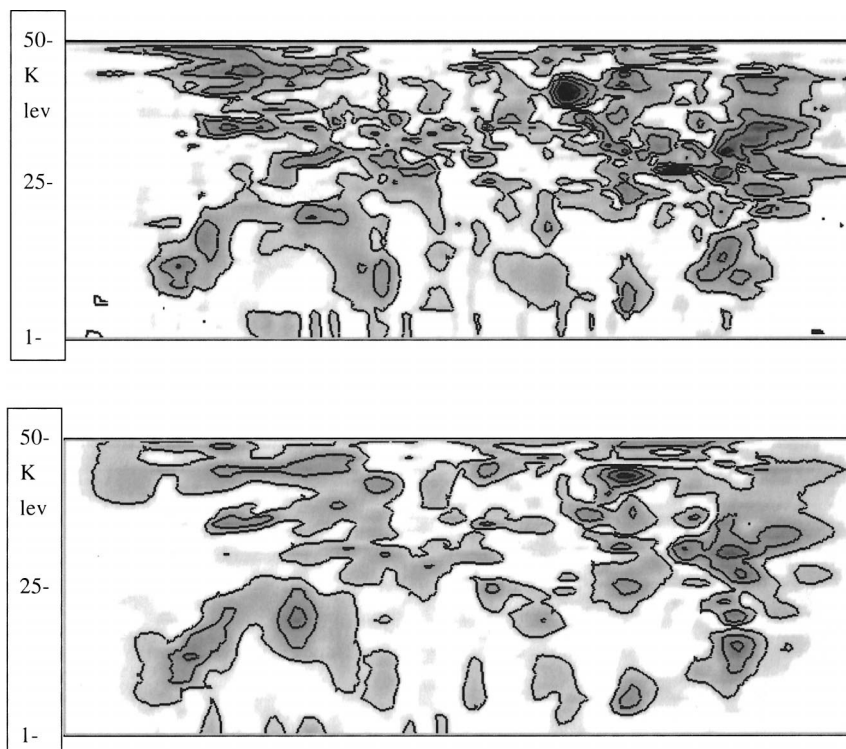
FIG. 7. Vertical cross section (west–east across RUC domain) of magnitude of vector wind (u and v) analysis increment for 1200 UTC 15 Jan 2002 using (a) OI analysis and (b) 3DVAR analysis. Contour interval is 2.0 m s^{-1}. Vertical axis is RUC native coordinate level (k), and horizontal orientation is west–east at approximately 40°N. Figure is used qualitatively only. Discontinuity near $k = 5$ is from use of surface data only through lowest 5 levels in OI analysis and mapping of native levels 1–4 into a single level in the 56-level 3DVAR solution.

has no isentropic or other coordinate dependencies. In the present version, the analysis is performed on a coarser-resolution horizontal grid (grid distance is 80 km), and the coarser-resolution analysis increment is interpolated back to the fine-resolution grid. This is a first step toward the introduction of a multigrid technique in the RUC 3DVAR.

In the multivariate mass/wind analysis step, balancing is provided by linear regression using regression coefficients computed from a history of previous RUC runs (6- and 12-h forecasts valid at the same time) using the so-called National Meteorological Center (NMC) method (Parrish and Derber 1992) in which forecast differences are used as a proxy for forecast errors to obtain correlations between streamfunction and balanced height. At present, no cross correlation between streamfunction and velocity potential is specified.

For most observation types, the observation operators are simply linear interpolation operators. The observation standard deviation errors (measurement and representativeness) are specified by diagonal matrices. The matrix values are obtained from corresponding values in the OI method.

The background error correlations are approximated by convex linear combinations of digital Gaussian filters with different filter scales, a method developed at NCEP [for details see Purser et al. (2001)]. Based on this filtering technique, approximate convolutions of a SOAR correlation function are obtained for different variables and vertical levels, and increment fields are computed. Present real-time computer time restrictions limit our scheme to two Gaussian filter applications in each space direction for each variable. Different numerical experiments were performed to obtain the optimal combination of filter weights. The full background error covariance matrix is applied in preconditioning (Derber and Rosati 1989). Minimization is accomplished using a simple conjugate gradient method.

c. Treatment of surface fields

The RUC 3D analysis is designed to produce an effective surface analysis, maintaining a close fit to the observations without introducing unwanted noise in the subsequent forecast. It uses all surface observations, including temperature, dewpoint, surface pressure, and winds (Table 2). By using a 1-h forecast background, it can provide consistency with dynamical, boundary layer, and land-use-related effects much better than that in a surface analysis using a persistence forecast back-

ground (Miller and Benjamin 1992). Operational regional models, including the RUC, currently use a horizontal resolution that resolves many terrain-related phenomena too small to be resolved by the current surface observation network in the United States. For this reason, many near-surface effects are accounted for in the RUC but not in persistence-based analyses, including sea/land/lake breezes, mountain–valley circulations, drainage winds, effects of variations in soil moisture, vegetation type, land use, roughness length, snow cover, land–water contrast, and cloudy/clear boundaries. Quality control (QC) is also improved for surface observations using a model background, since the model provides an independent assessment of surface conditions and is, therefore, better able to identify errors repeated every hour at a given station than a persistence-based QC. The RUC analysis is also able to provide full dynamical consistency through coastal regions as opposed to the persistence approach, which requires blending with an external model in these areas (Fig. 3 of Miller and Benjamin 1992).

As described in Devenyi and Benjamin (2003), all station pressure (altimeter) and surface wind observations are used regardless of the difference between station and model elevation. The station pressure is reduced to the model elevation using the local lapse rate over the bottom five levels in the background field (approximately 20–25 hPa). Temperature and dewpoint observations are reduced, via the local lapse rate, from actual station elevation to model terrain height, provided that the reduction does not exceed 70 hPa. Fewer than 15 surface stations reporting within the RUC domain (as of early 2003) do not meet this criterion, resulting in discarding their temperature and dewpoint values.

Finally, the output fields of 2-m temperature and dewpoint from the RUC are the result of a further step in postprocessing to a special terrain elevation field designed to match elevations of surface stations (Benjamin et al. 2002a). This procedure is essentially the inverse of the forward model for surface observations of temperature and dewpoint referred to in the previous paragraph. This step allows RUC analyses of 2-m temperature and dewpoint to more closely match observations.

d. Cloud/hydrometeor analysis using GOES cloud-top data

The RUC model produces explicit forecasts of mixing ratios of cloud water, rainwater, ice, snow, and graupel through a mixed-phase bulk cloud microphysics parameterization (Benjamin et al. 2004). These variables are all cycled through the RUC assimilation cycle, as shown in Table 3. Toward the goal of improved short-range forecasts of cloud/hydrometeors, icing, and precipitation, a technique for assimilating GOES cloud-top pressure/temperature data from single fields of view was introduced into the operational RUC in 2002 with the 20-km version. This technique is described in greater

detail by Benjamin et al. (2002b) and Kim and Benjamin (2001). The previous RUC 1-h forecast provides a background for these hydrometeor fields, and the cloud analysis includes both clearing and building, starting with the background fields. GOES cloud-top pressure gives information on the presence or absence of clouds, but not on cloud depth. Also, unless the top cloud layer is broken, the cloud-top pressure cannot provide information on multiple cloud layers. Thus, the RUC cloud/hydrometeor assimilation technique is designed to use this incomplete information. Where GOES data indicate absence of clouds, the technique removes any hydrometeors and reduces water vapor mixing ratio to a subsaturation value. Where GOES data indicate the presence of clouds that are not in the RUC 1-h forecast, cloud water and/or ice is added in a layer not exceeding a 50-hPa depth. The water vapor mixing ratio in this layer is saturated. Ice saturation is assumed for temperature below 248 K and water saturation for temperatures above 263 K. In between these values, the saturation vapor pressure varies linearly between the value for ice at 248 K and the value for liquid water at 263 K. If the GOES retrieved cloud-top pressure is greater than 620 hPa, the cloud-top pressure is rederived using both the GOES cloud-top temperature and the RUC 1-h temperature profile at the nearest grid point. The median values from the fields of view around each RUC grid box are used. Cloud fraction is calculated with this sampling into RUC grid volumes for later use in cloud building/clearing criteria. The RUC cloud assimilation includes safeguards to prevent level-assignment problems with convective and marine stratus clouds, as described by Benjamin et al. (2002b).

e. Quality control of observations

Observation quality control in the RUC is primarily based on a buddy check between neighboring observations. Before buddy check or other quality control procedures proceed, gross quality control tests (range limits, wind shear, lapse rate) are applied to all observations. The buddy check considers observation innovations, the differences between the observation and the background field interpolated to the observation point [$\mathbf{d}_i$ in Eq. (5), section 2], instead of the observations alone. This is an important distinction since it means that any known anomaly in the previous forecast has already been subtracted out, improving the sensitivity of the QC procedure to actual errors. The RUC buddy check is based on an optimum interpolation method whereby an estimate at the observation point is made from the innovations of a group of up to eight nearby ''buddy'' observations, similar to that described by Benjamin et al. (1991). If the difference between the estimated and observed innovations exceeds a predefined threshold, the observation is flagged. For each observation, the QC check is repeated, removing one of the buddies at a time to increase the robustness of the check.

Because the RUC utilizes a partially flow-dependent adaptive (quasi isentropic) background error structure, its buddy check method has some adaptivity. As pointed out by Dee et al. (2001), another option to the adaptive buddy check is the application of locally adjusted thresholds. Locality and adaptivity of the buddy check ensures that the efficacy of quality control is less dependent on global approximations introduced into the parameterization of the optimum interpolation scheme. Isolated observations where no buddies are available are flagged if their innovation exceeds a variable-dependent multiple of the background error.

Checks are also made for contamination of VAD and profiler wind observations due to bird migration. Prior to dissemination of the data, a careful check for bird (and other) contamination in profiler winds is made at the Profiler Hub in Boulder, Colorado. This check includes use of second-moment data to examine likelihood of bird contamination. If the quality control flag produced by this check indicates suspicious data, the profiler data at that level are not used. For VAD winds, no second-moment data are available, so a more conservative check is made. A solar angle is calculated, and if the sun is down and the temperature is higher than $-2°C$, VAD winds are not used if they have a northerly component between 15 August and 15 November or a southerly component between 15 February and 15 June.

5. Verification—Analysis and forecast fit to rawinsonde and surface observations

The purpose of the Rapid Update Cycle is to use more recent observations to produce more accurate short-range forecasts than would otherwise be available. The RUC is unique in its operational use of a very high-frequency intermittent assimilation cycle (3-h intermittent assimilation cycle from 1994 to 1998 and a 1-h cycle from 1998 to present). While the use of more recent observations should lead to improved short-range forecasts, it is not a foregone conclusion that shorter-range forecasts will be more accurate than longer-range forecasts valid at the same time. If observations are available at an update time but are very sparse and introduce substantial aliasing (discussed in section 2b), the shorter-range forecast will likely be worse than the longer-range forecast at the same time. If wind-only observations are available and inadequate provision is made in the assimilation to produce a sufficiently balanced wind/mass increment, it is again likely that the short-range forecast will be worse than the longer-range forecast. Whether or not this is so depends on the amount, quality, and 3D spatial coverage of the high-frequency observations, and the assimilation techniques used. Of course, in the absence of any high-frequency observations, a short-range forecast will provide no improvement over a longer-range forecast (e.g., a 3-h forecast initialized with no additional observations is equivalent to a 6-h forecast valid at the same time).

The mix of high-frequency (approximately hourly) observations available over the United States (Table 2) provides generally irregular and incomplete coverage. Except for the profiler observations, wind observations tend to be in the upper troposphere (aircraft; some cloud drift) and in the lower troposphere (VAD; surface). Aircraft ascent/descent profiles occur at least every 3 h near only about 20 airport hubs. Frequent temperature observations are limited to aircraft and surface observations. Frequent moisture observations are only for vertically integrated totals above the surface. Rawinsondes provide a more complete network spatially (horizontally and vertically) and include all basic variables (wind, temperature, height, moisture) in full profiles, but are "low frequency" observations, generally available only near 0000 and 1200 UTC.

In the two sections below, verification statistics are presented for RUC forecasts of different durations against observations from rawinsondes and surface reporting stations. Before starting, we note two aspects about these statistical measures of short-range forecast improvement. First, overall statistics mask much stronger differences that may occur in individual cases. Second, though the statistics here may be legitimately intercompared since they use the same verifying observations and time period, it is problematic to compare these with other sets of verification statistics over different time periods, different domains, different observations, or even different quality control standards for those observations.

a. Upper-air verification against rawinsondes

Before considering forecast accuracy, observation fit statistics for both OI and 3DVAR versions of the RUC analysis (Fig. 8) for a period in November–December 2002 are first presented. This is one method to evaluate the performance of the analysis procedures. Assumed errors for rawinsonde observations are generally about $2.5–4$ m s^{-1} for wind, $0.5°C$ for temperature, $5–10$ m for height (increasing with altitude above the surface), and the equivalent of about 8% for relative humidity. [A collocation study of rawinsonde and aircraft observations by Schwartz and Benjamin (1995) gives limits on observation errors.] As expected, the fit to rawinsonde observations generally corresponds to these values. It may also be noted that this fit to the observations is closer than that for the 1-h forecast shown in Fig. 9. It is also apparent in Fig. 8 that the fit to observations is comparable between the 3DVAR analysis and the OI analysis. The slightly closer fit from 3DVAR is an inadvertent effect, resulting from the tuning of background error in the 3DVAR analysis to produce an optimal 3-h forecast skill.

Evaluation of the overall accuracy of RUC forecasts of wind, height, temperature, and relative humidity from projections of different durations (1, 3, 6, 9, 12 h) is presented in Fig. 9 for a period of almost 4 months from
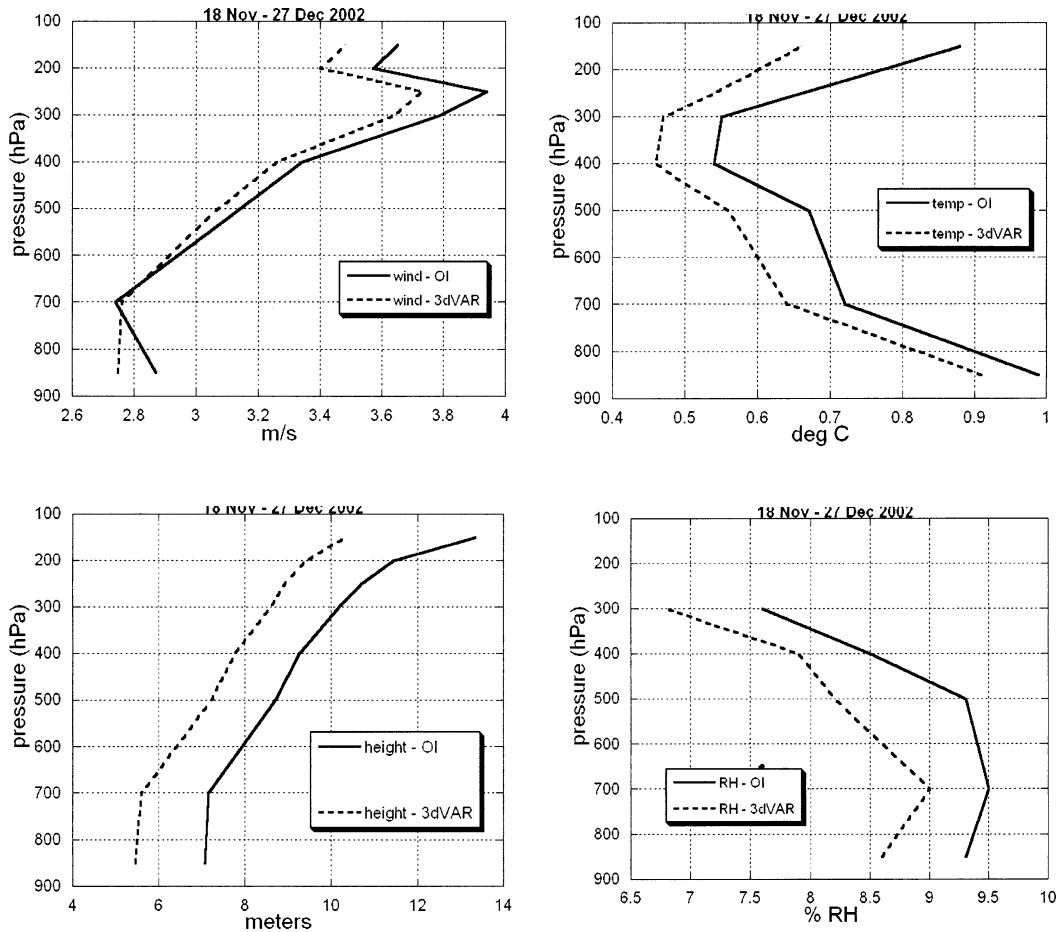
FIG. 8. RUC analysis fit to rawinsonde observations for both optimal interpolation and 3D variational versions for the period from 18 Nov to 27 Dec 2002, using NCEP rawinsonde quality control flags. Rms vector difference or standard deviation difference between observations and analyses: (a) wind (m s^{-1}), (b) height (m), (c) temperature (°C), and (d) relative humidity (% RH). All verification using 40-km gridded data postprocessed from the 20-km RUC.

September to December 2002 using an OI-based cycle. Skill for 3- and 12-h RUC forecasts verified against rawinsonde observations has been shown to be nearly identical from a 3DVAR-based cycle (results not shown). This verification is performed using rawinsonde observations as "truth"; the forecast-minus-observation differences, labeled as "errors," in fact include *both* forecast and observational error. Generally, the RUC is successful in producing shorter-range forecasts that are more accurate than those of longer duration. For both wind (Fig. 9a) and temperature (Fig. 9c), this trend is apparent in forecasts all the way down to a 1-h forecast at almost every mandatory pressure level. In other words, 9-h forecasts are statistically more accurate than 12-h forecasts, and even 1-h forecasts are more accurate than 3-h forecasts. For height forecasts (Fig. 9b), shorter-range forecasts show general improvement over 12-h forecasts, but 1-h forecasts at some levels (e.g., 700 hPa) show less accuracy than 3-h forecasts. This is presumably due to residual mass/momentum imbalance despite the balancing in the analysis increment calculation

and application of the digital filter assimilation (section 2a). A slight improvement of relative humidity forecasts (Fig. 9d) at shorter range is evident at 700 and 300 hPa, but some degradation is shown at 500 and 850 hPa. Recent data sensitivity experiments by Smith et al. (2003) suggest that allowing precipitable water observations to influence levels as high as 500 hPa in winter may produce degraded short-range forecasts at this level, but more research is needed on this topic.

A forecast percentage improvement for an *x*-h forecast over 12-h forecast skill is calculated as

$$\Delta \text{ improvement} = 100 \frac{\sigma_{f-12h} - \sigma_{f-x}}{\sigma_{f-12h} - \sigma_a}, \qquad (11)$$

where σ_{f-12h}, σ_{f-x} are rms or standard deviation errors for 12- and *x*-h forecasts, respectively, and σ_a is the analysis fit to observations (considered equivalent to a perfect forecast, accounting for observation error). A 100% score here corresponds to a perfect forecast, and 0% means no improvement over 12-h forecast skill. The
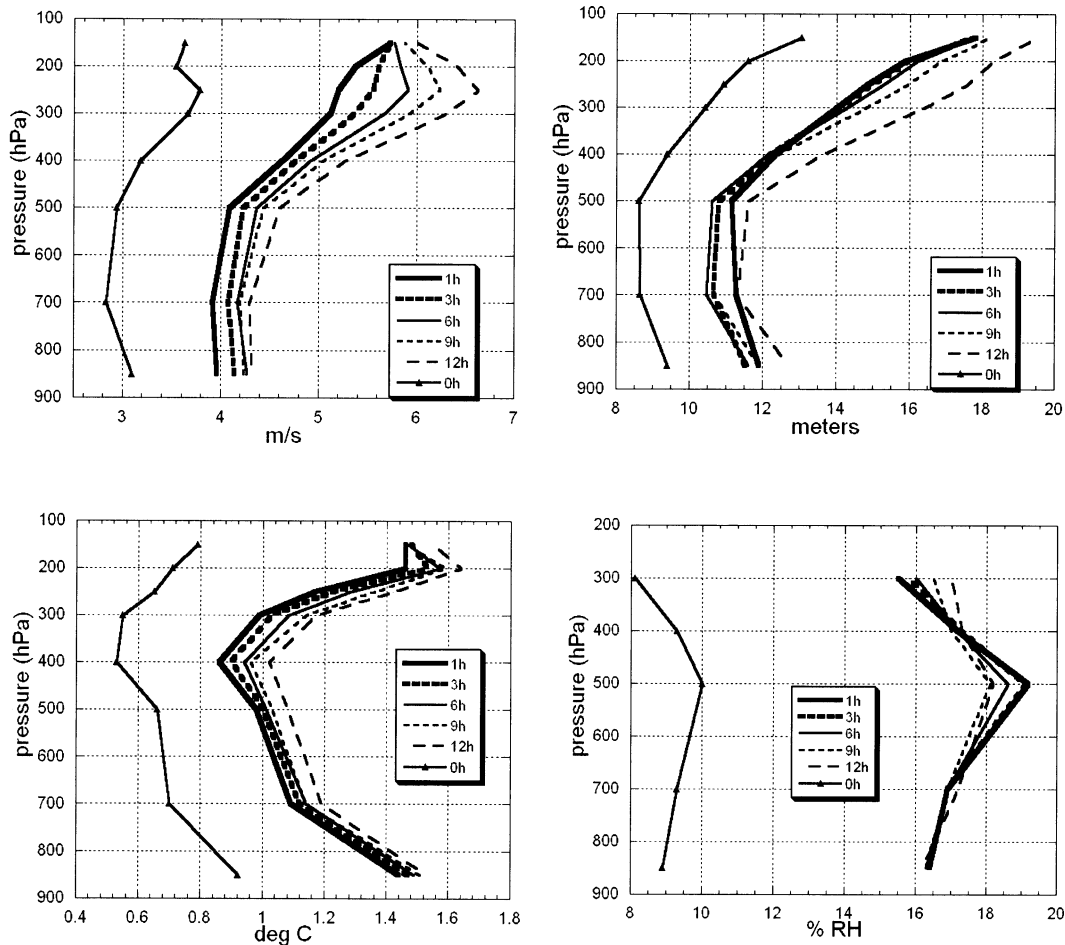
FIG. 9. Verification of RUC forecasts against rawinsonde observations over entire RUC domain. For the period 11 Sep–31 Dec 2002, using NCEP rawinsonde quality control flags. Rms vector difference or standard deviation difference between observations and forecasts is shown for forecasts of 1-, 3-, 6-, 9-, and 12-h duration and for the analysis, all valid at rawinsonde observation times (0000 and 1200 UTC): (a) wind (m s^{-1}), (b) height (m), (c) temperature (°C), and (d) relative humidity (% RH). All verification using 40-km gridded data postprocessed from the 20-km RUC. Note that zero line does not correspond to the left-hand side in these graphs.

percentage improvement of RUC 1-, 3-, 6-, and 9-h forecasts has been evaluated from the same 4-month set of RUC forecasts described in the previous paragraph and plotted in Fig. 10. The percentage reduction of 1-h forecast error over 12-h forecast error reaches as high as 50% at jet level for winds, and over 30% for temperatures. For heights, the projection showing the most improvement over 12-h forecasts averaged over all levels is the 6-h forecast, which reduces error by 30% at all levels except 150 hPa. Relative humidity short-range forecasts range from −10% to +10%, as discussed in the last paragraph.

Overall, with some exceptions, the RUC appears to accomplish its goal of providing improved short-range guidance using high-frequency assimilation for conditions above the surface. The statistical verification of RUC forecasts down to the cycle period (1 h) appears to provide a reasonable measure of the effectiveness of

the high-frequency assimilation. For winds and temperatures, the 1-h cycle is clearly effective in providing improved background forecasts for each analysis. Figures 9 and 10 indicate that there may be issues in assimilation of surface pressure and moisture observations. These will be addressed in ongoing research toward the goal of further improving overall short-range RUC forecast skill.

An example of the progression of improved forecasts at shorter forecast projections is presented in Fig. 11. Forecast-minus-analysis differences for 250-hPa wind forecasts valid at 0000 UTC 27 January 1998 are shown for 12-, 9-, 6-, and 3-h forecasts. The overall magnitude of the estimated error decreases as the projection decreases. However, the forecast improvement is not linear in space or time but is dependent on where and when observational data are available. For instance, the skill of the forecast over southern California is not improved
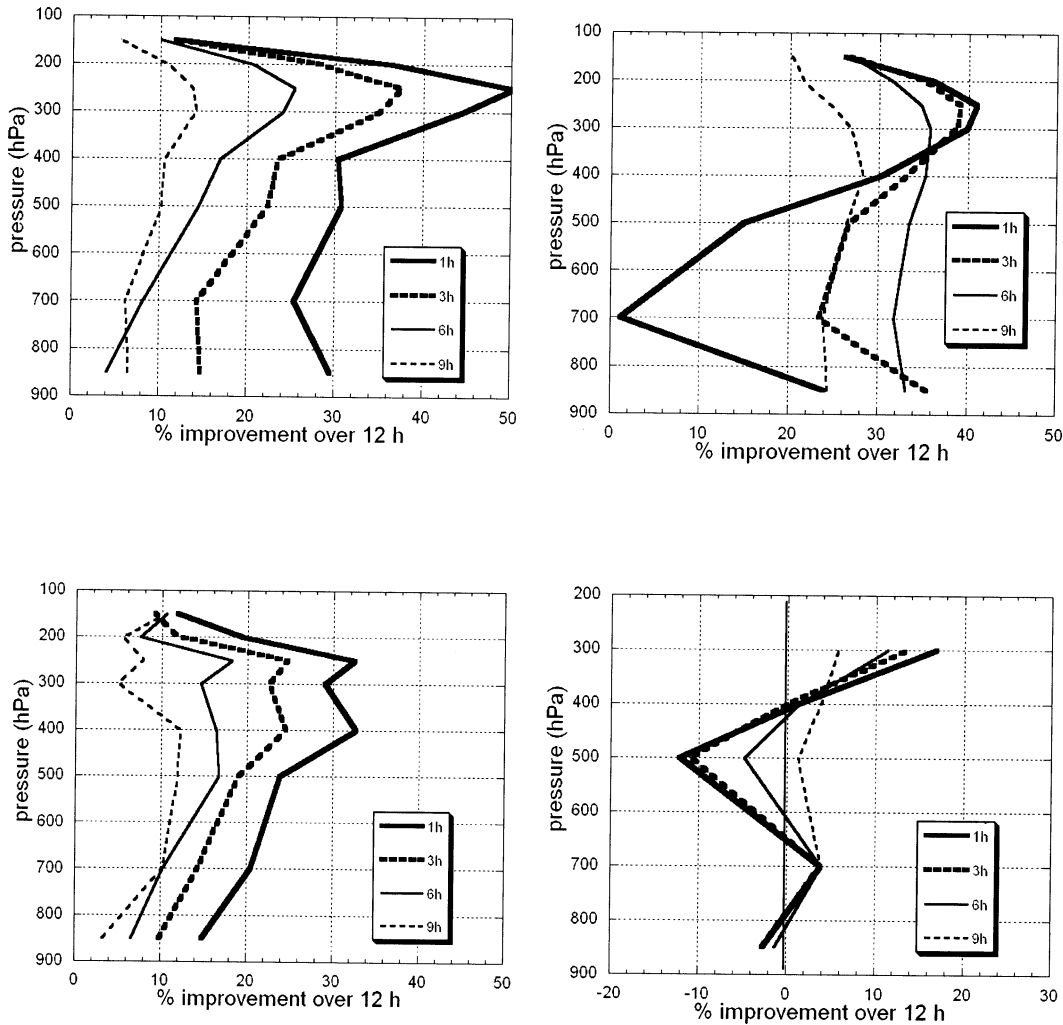
FIG. 10. Percentage improvement of 1-, 3-, 6-, and 9-h RUC forecasts over 12-h RUC forecasts valid at the same time. Same period and variables as in Fig. 9.

until some data are assimilated between 1800 and 2100 UTC, resulting in an improved 3-h forecast over the previous forecasts.

A strong test for any short-range model forecast system to beat is a corresponding persistence forecast of the same duration. A comparison of RUC 1- and 3-h model forecast with 1-h persistence forecast skill is presented in Fig. 12. It was found that RUC 1-h model forecasts actually provide improved skill over corresponding 1-h persistence forecasts for all variables and levels except for heights in the lower troposphere and relative humidity at 300 hPa. For wind and temperature, 3-h model forecasts had approximately the same skill as 1-h persistence forecasts. This result suggests that the time representativeness and windowing issues discussed in section 2b are significant and that even the RUC 1-h cycle might gain some benefit from using an FGAT (section 2b) background for observations distributed over time within a 1-h window.

Verification of RUC forecasts out to 24-h duration has also been performed for the same 4-month period in 2002 from runs at the FSL. The operational RUC at NCEP currently produces forecasts only to 12 h, as shown in Fig. 1, but experimental RUC forecasts out to 48 h have been produced experimentally at FSL daily since late 2000. Even though the operational niche assigned to the RUC is currently limited to 12-h forecasts, the RUC prognostic model is fully capable from the standpoint of conservation properties and physical parameterizations of running much longer forecasts. Examples of 36-h RUC forecasts at 20- and 10-km resolutions are presented in Benjamin et al. (2004). Results from RUC 24-h forecast verification are presented in Fig. 13, along with 12-h model and 3- and 12-h persistence forecast errors, again relative to rawinsonde observations. They show that the increase of forecast error from 12 to 24 h is modest for all four variables shown, up to 1.6 m s^{-1} for wind and 4 m for height at
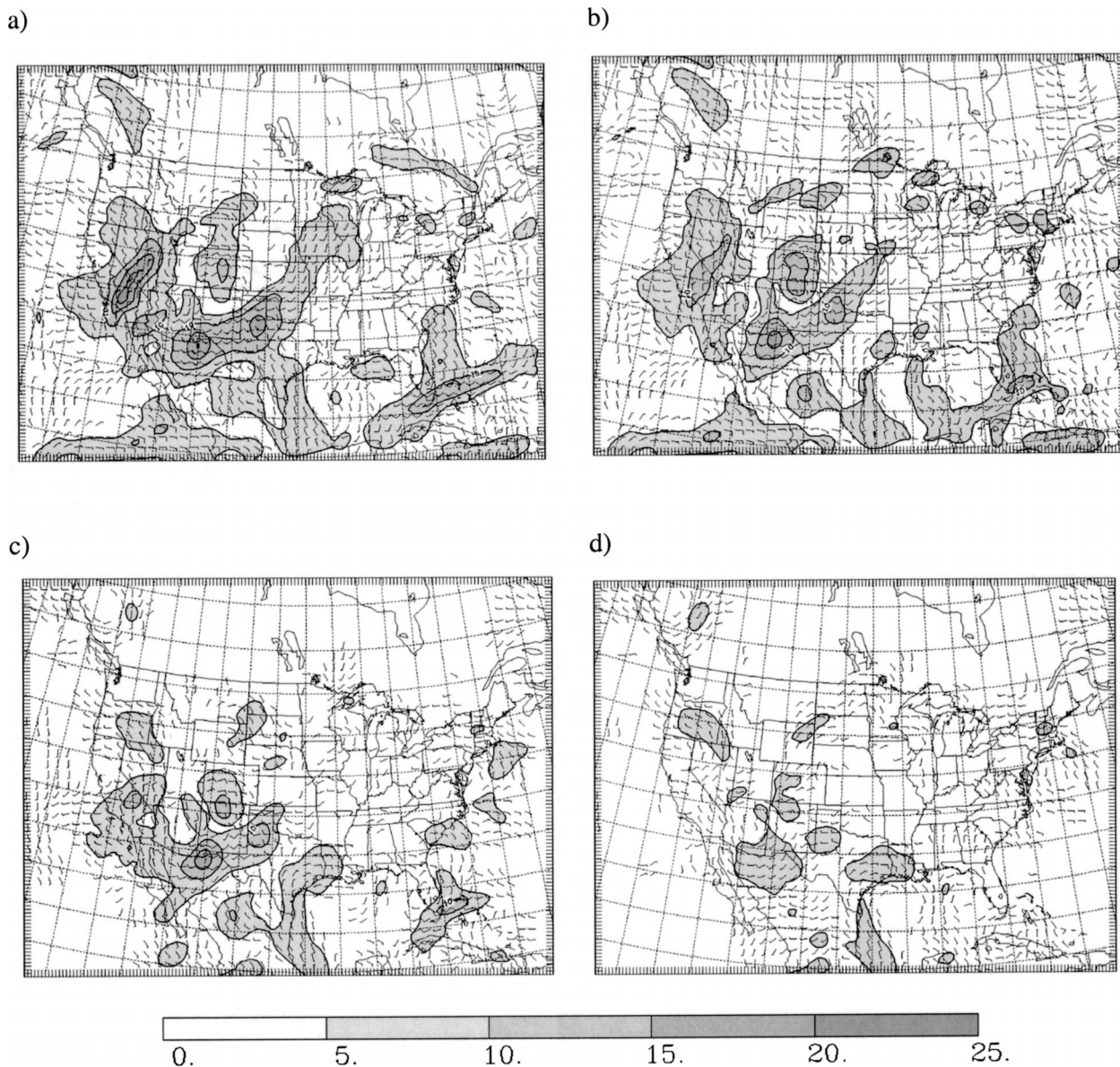
a)

b)

c)

d)

FIG. 11. RUC20 forecast vector difference from verifying analysis (forecast minus analysis) for 250-hPa wind forecasts valid 1200 UTC 8 Feb 2001: (a) 12-h forecast initialized at 0000 UTC 8 Feb, (b) 9-h forecast initialized at 0300 UTC, (c) 6-h forecast initialized at 0600 UTC, and (d) 3-h forecast initialized at 0900 UTC. Units in m s^{-1}.

200–300 hPa, and up to 0.4°C for temperature and 3% for relative humidity. Moreover, the 24-h RUC forecast errors are far smaller than 12-h persistence errors (about 40%–60% of 12-h persistence forecast errors) for the period shown for all variables. The persistence errors shown in Fig. 13 indicate the strong variability of the atmosphere over 12-h periods and even over 3-h periods for the RUC domain for this period. The 3-h persistence forecast error exceeds 12-h RUC forecast error for all variables and levels and approximates the 24-h RUC forecast error for winds and heights at 300–500 hPa and RH at all levels. The levels of peak persistence error indicate the levels of strongest change: at jet levels for

winds and heights, at tropopause level and near the surface for temperature, and in the middle troposphere for relative humidity, showing the strong control by vertical motion.

b. Surface verification

The accuracy of RUC near-surface forecasts is strongly dependent on the treatment of the land surface and boundary layer in the RUC forecast model. These treatments are described in detail in the companion paper on the RUC model (Benjamin et al. 2004). Verification of RUC surface forecasts was performed using all sur-
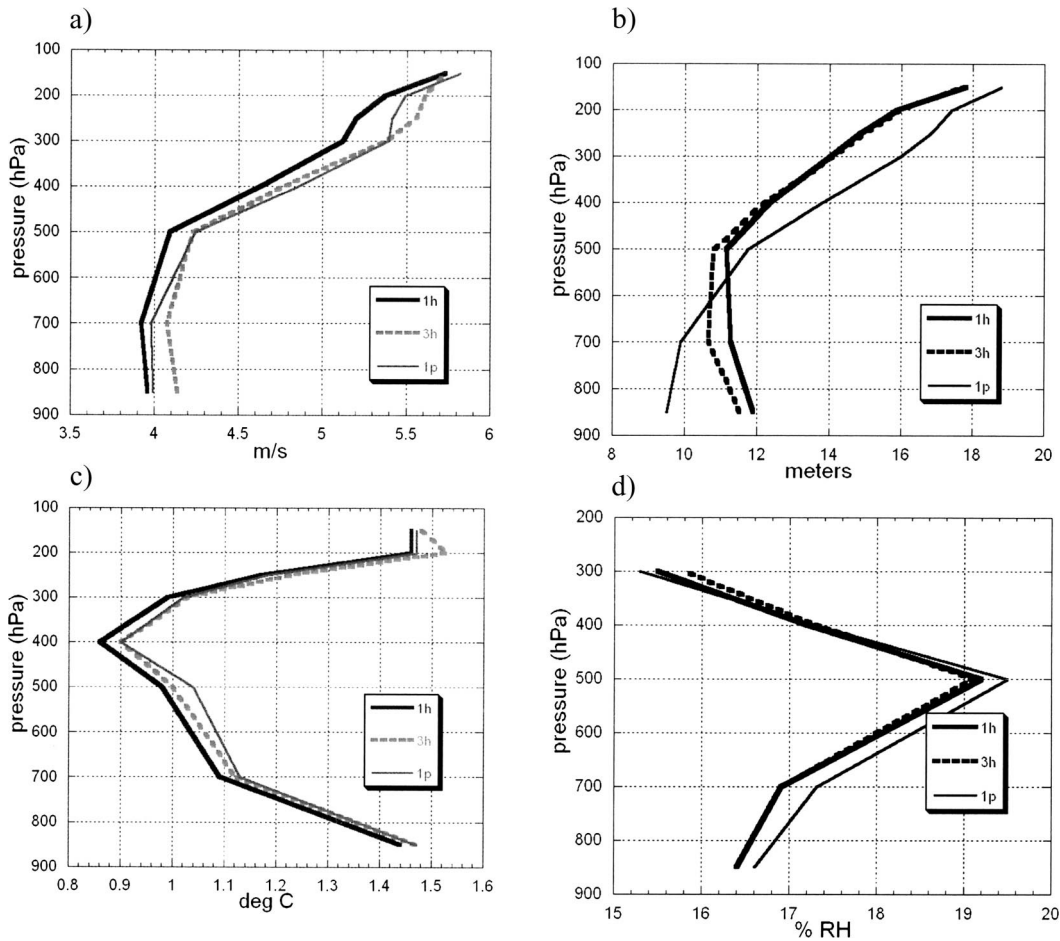
FIG. 12. Verification of 1- and 3-h RUC model forecasts vs 1-h persistence (1p) forecast, all valid at the same time. Same period and variables as in Fig. 9.

face meteorological aviation report (METAR) observations available within the RUC domain. (No QC was performed for verifying observations, resulting in some inflation of error statistics over those if screening had been performed.) Forecasts of four different surface variables were verified: 10-m wind speed (Fig. 14), 10-m wind vector (Fig. 15), 2-m temperature (Fig. 16), and 2-m dewpoint temperature (Fig. 17). The RUC gridded values of 2-m temperature and dewpoint temperature are reduced to a special terrain elevation as described in section 4c and Devenyi and Benjamin (2003). Every 3 h, differences were calculated between METAR observations and RUC analyses and forecasts of different durations. Statistics are presented separately for a warm-season period (April–September 2002) and a cool-season period (October–December 2002). All RUC grids were from the FSL backup version of the 20-km RUC, which used code nearly identical to the NCEP operational version during this period except for the assimilation of extra observations not yet available at NCEP, including those from surface mesonetworks, GPS precipitable water retrievals, and boundary layer profilers.

In addition, the 20-km grids were first thinned to a 40-km grid, and then grid values were bilinearly interpolated to METAR locations from the 40-km grid. Our experience is that 20-km (full resolution) surface grids frequently show improved depictions of local circulations versus 40-km grids, although 20- and 40-km *forecast* grids (derived from the 20-km model) verify statistically against observations equally well. For *analyses,* the statistical fit to observations is closer using 20-km grids compared to the 40-km grids.

RUC 10-m wind forecasts were verified both for wind speed difference (Fig. 14) and vector magnitude difference (Fig. 15) from METAR observations. The rms fit for wind speed to METAR observations is 1.5 m s^{-1}, increasing to 1.75 m s^{-1} at a 1-h projection, and 2.0 m s^{-1} at 12-h forecasts (Fig. 15). For verification using *vector* wind differences between forecasts and observations, the magnitudes are somewhat larger (generally about 3.75–4.0 m s^{-1}) because they incorporate direction differences. These differences are smaller than those for rawinsonde wind observations aloft (Fig. 9), which may be expected, in part, since surface winds are
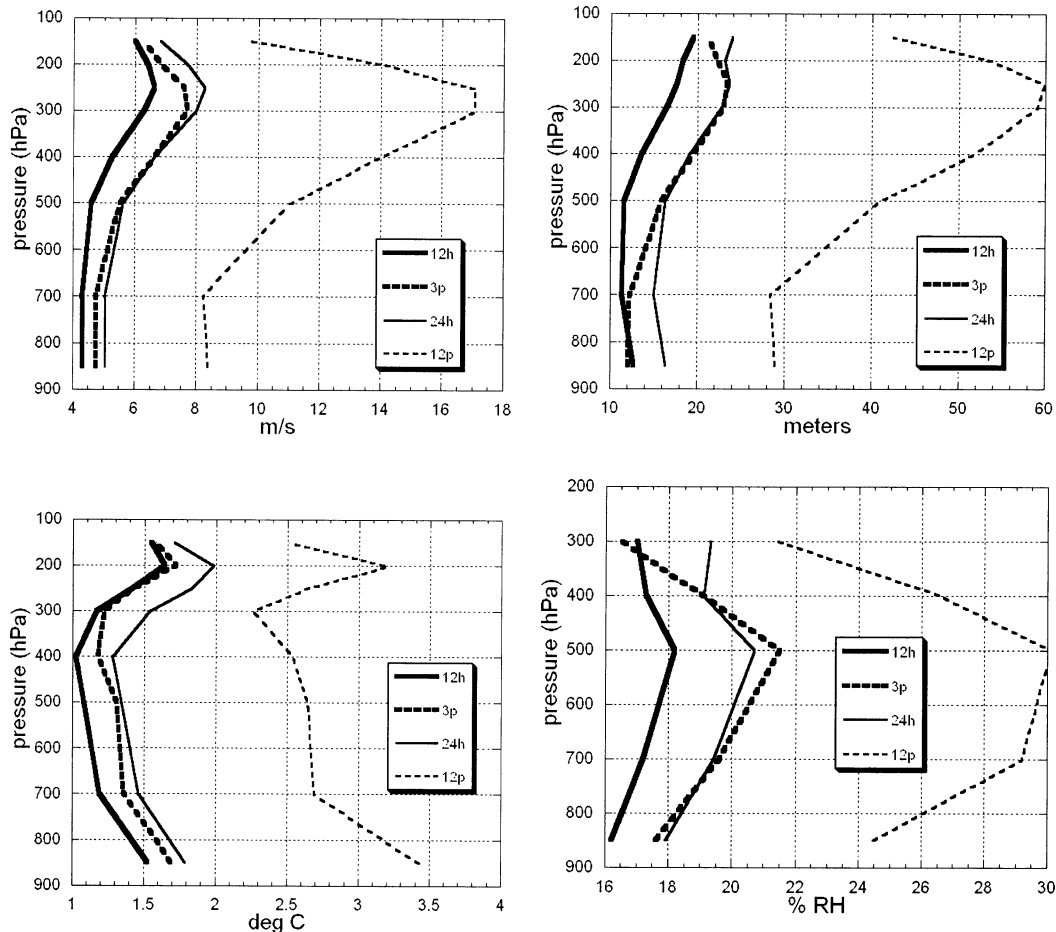
FIG. 13. RUC 12- and 24-h model forecast error and 3- and 12-h persistence error, all valid at the same time, verified against rawinsonde observations for the same period and variables as in Fig. 9.

generally lighter than winds aloft. For both wind speed and vector wind verification, RUC forecasts show increasing skill at shorter range. Moreover, both 1- and 3-h 10-m wind speed and vector RUC model forecasts show improved skill on average over 1- and 3-h persistence forecasts, respectively (Figs. 14, 15). The improvement over persistence for surface winds is larger at 3 h than at 1 h.

Verification of 2-m temperature (Fig. 16) and dewpoint temperature (Fig. 17) forecasts also show that shorter-duration RUC forecasts are more accurate than longer-duration forecasts and provide added value, even for 1-h forecasts. Again, 1- and 3-h prognostic forecasts for 2-m temperature and dewpoint show improvement over respective persistence forecasts, albeit less so than wind forecasts, especially for dewpoint forecasts, which show only slightly higher skill than corresponding persistence forecasts. On the other hand, 2-m temperature and dewpoint forecasts show a more steady improvement in forecast skill out to 12 h, in contrast to 10-m wind forecasts with only relatively small improvement in forecast skill between 3 and 12 h.

RUC surface forecast skill was also stratified into day (1500, 1800, 2100, and 0000 UTC) verification times versus those at night (0300, 0600, 0900, and 1200 UTC; not shown). Wind observation–forecast differences are larger in daytime, presumably since 10-m wind speed itself is generally higher in daytime because of boundary layer mixing. Surface temperature and dewpoint verification shows the same pattern for the summer period: larger observation–forecast differences in daytime. However, temperature differences in the cool-season period are slightly larger at night. Other surface verification results from the 20-km RUC are presented by Schwartz and Benjamin (2002).

6. Conclusions and plans

The Rapid Update Cycle is a 1-h assimilation/forecast cycle that runs on a 1-h cycle at the National Centers for Environmental Prediction to produce frequently updated 3D mesoscale analyses and short-range forecasts over the lower 48 United States and adjacent areas. The RUC is effective in its goal of providing more accurate
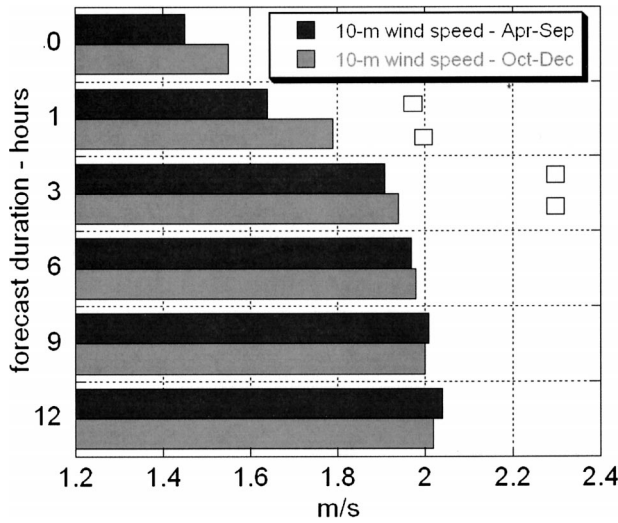
FIG. 14. Verification of RUC 10-m wind speed forecasts against METAR observations over full RUC domain. Value (m s⁻¹) is rms of observation–forecast difference. Two seasons are shown: 17 Apr–27 Sep 2002 and 1 Oct–26 Dec 2002. Values are shown for RUC forecasts of 1-, 3-, 6-, 9-, and 12-h duration, all valid at the same time. Open squares are rms difference for 1- and 3-h persistence forecasts using RUC analysis for each season.
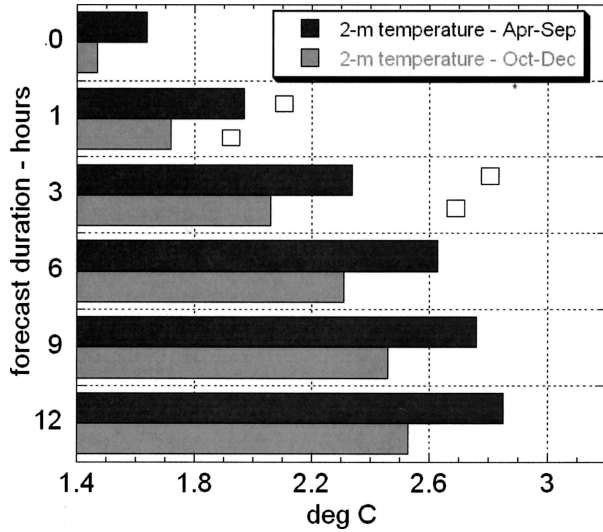

FIG. 16. Same as Fig. 14, but for 2-m temperature and standard deviation difference between METAR observations and RUC forecasts. Units are °C.

short-range forecasts initialized with recent data than longer-range forecasts verifying at the same time. This is the goal, of course, of any assimilation cycle, even on a 12-h frequency, but the RUC is unique in that it runs on a 1-h cycle and is successful in providing improved forecasts down to this projection. For all variables and levels except heights at 850 and 700 hPa, the RUC 3- and 1-h model forecasts are more accurate than corresponding 3- and 1-h persistence forecasts, on the average, over a 4-month evaluation period.

Challenges to the effectiveness of a 1-h intermittent assimilation cycle include the adequacy of observational

data to sufficiently resolve 1-h forecast error, the ability of the forecast error covariance model to effectively project these observations onto the true forecast error, and the requirement that the numerical model produce a well-balanced 1-h forecast without significant mass/momentum adjustment. These issues were discussed, including idealized experiments to understand the effects of time windowing on assimilation of aircraft data and other data of opportunity not provided by a regular network. The strategies used in the RUC to address these issues include application of a digital filter initialization and an adaptive forecast error covariance model set in a quasi-isentropic vertical coordinate.

As of early 2003, the operational RUC runs at 20-km horizontal resolution and with 50 vertical levels. A
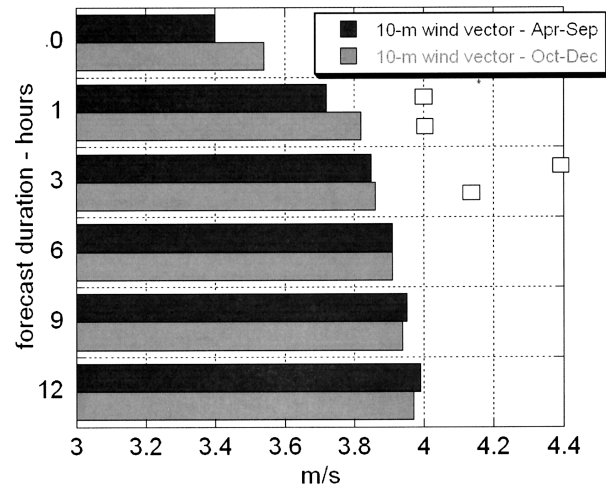

FIG. 15. Same as Fig. 14, but for 10-m rms vector wind difference between METAR observations and RUC forecasts. Units are m s⁻¹.
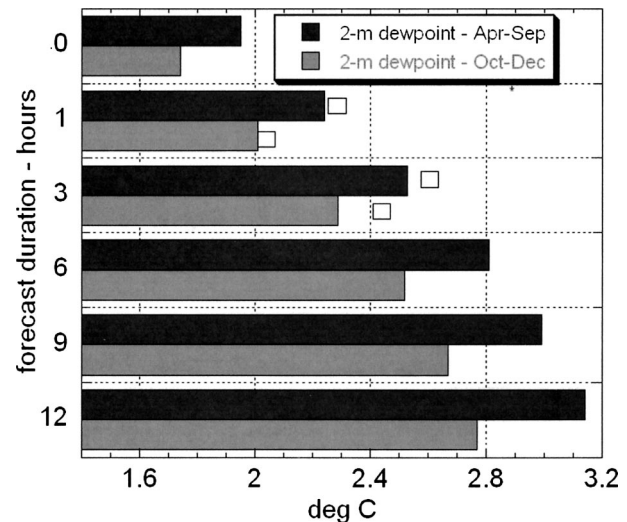

FIG. 17. Same as Fig. 16, but for 2-m dewpoint temperature (°C).

hybrid isentropic–terrain-following vertical coordinate is used in both the RUC analysis and the RUC prediction model, described in detail in a companion paper (Benjamin et al. 2004). A unified analysis framework allowing solutions from either optimal interpolation or three-dimensional variational techniques has been developed for the RUC. The unified analysis framework uses a generalized coordinate approach, currently set as the hybrid quasi-isentropic coordinate but capable of accommodating other vertical coordinate systems as well. The RUC analysis assimilates rawinsonde observations and a full range of high-frequency observations, including those from commercial aircraft, wind profilers, VAD wind profiles from radar, satellite retrievals of precipitable water and cloud-drift winds, GPS ground-based precipitable water retrievals, and surface stations. Although a wide variety of observation types are assimilated into the RUC, the high-frequency coverage is irregular and often quite sparse in space and time even over the RUC domain. An initial cloud analysis, using GOES cloud-top pressure/temperature data to clear and build cloud (modifying 3D hydrometeor mixing ratios and water vapor mixing ratio from the RUC 1-h forecast background field), is also included in the RUC analysis.

Extensive verification over multimonth periods of RUC forecasts against rawinsonde and surface METAR observations has been presented. This verification shows that the ability of the RUC to use irregularly distributed high-frequency observations to provide improved forecasts aloft at increasingly shorter durations is most evident for wind and temperatures, where an increase in skill is shown down to a 1-h forecast at all mandatory levels. For heights, 6-h RUC forecasts show a strong improvement over 12-h forecasts valid at the same time, but 1- and 3-h forecasts do not in the lower troposphere. For relative humidity forecasts, this ability for improved short-range forecasts is mixed, certainly in part because of an absence of in situ high-frequency moisture observations over the United States except at the surface. One-hour RUC forecasts are shown to provide a 15%–30% reduction of 12-h temperature forecast error over a layer from 850 to 200 hPa and a 25%–50% reduction of 12-h wind forecast error over the same layer. Short-range RUC forecasts of 2-m temperature and dewpoint temperature and 10-m wind also show an increase in skill down to a 1-h forecast over longer-range forecasts valid at the same time. For both forecasts aloft and at the surface, the RUC short-range forecasts show a strong improvement over corresponding persistence forecasts at 3-h and even at 1-h projections, a difficult test for numerical forecast models at such a short range. Wilson et al. (1998) presented a recent diagram with a qualitative depiction of the applicability of different forecasting techniques, including models, extrapolation, and expert systems for very short-range forecasts, to the problem of forecasting convective storm evolution. The predictability of phenomena is dependent on the life cycle duration of that phenomenon,

and the life cycle of thunderstorms is certainly on a shorter time scale than that of the phenomena generally responsible for changes in surface and upper-air atmospheric measurements used in the RUC forecast verification shown in this paper. On the other hand, the challenge for the RUC is to use irregularly spaced and usually sparse observations to extract a net improvement in forecast skill, which it is able to do. Verification of RUC 24-h forecasts is also presented from a 4-month period, showing modest growth of error from 12 to 24 h and that 24-h RUC model forecast skill approaches that of a 3-h persistence forecast.

The operational RUC analysis changed from an OI to a 3DVAR analysis on 27 May 2003. Other plans over the next two years include introduction of improved cloud/hydrometeor analysis techniques, including assimilation of radar assimilation and surface cloud and current weather observations, recalculation of forecast background error covariances, testing of a *diabatic* digital filter initialization (Huang and Lynch 1993), and revised techniques for assimilation of all surface observations. Improved assimilation of radar and satellite-based observations will be introduced, especially to strengthen short-range forecasts of precipitation. The RUC will also move to higher horizontal resolution, with a planned upgrade to 12–15-km resolution in 2004 or 2005.

The Rapid Update Cycle will make a transition to a version based on the Weather Research and Forecast (WRF) Model and assimilation system (e.g., Skamarock et al. 2001) over the next several years. The techniques found to be essential for effective high-frequency assimilation in the current Rapid Update Cycle will be incorporated, as necessary, into WRF-based versions of future operational rapid updating assimilation and forecast systems that will be descendants of the current RUC.

REFERENCES

Barwell, B. R., and A. C. Lorenc, 1985: A study of the impact of aircraft wind observations on a large-scale analysis and numerical weather prediction system. *Quart. J. Roy. Meteor. Soc.,* **111,** 103–129.

Benjamin, S. G., 1989: An isentropic mesoα-scale analysis system and its sensitivity to aircraft and surface observations. *Mon. Wea. Rev.,* **117,** 1586–1605.

——, K. A. Brewster, R. L. Brummer, B. F. Jewett, T. W. Schlatter, T. L. Smith, and P. A. Stamus, 1991: An isentropic three-hourly data assimilation system using ACARS aircraft observations. *Mon. Wea. Rev.,* **119,** 888–906.

——, K. J. Brundage, P. A. Miller, T. L. Smith, G. A. Grell, D. Kim, J. M. Brown, and T. W. Schlatter, 1994: The Rapid Update Cycle at NMC. Preprints, *10th Conf. on Numerical Weather Prediction,* Portland, OR, Amer. Meteor. Soc., 566–568.

——, and Coauthors, 2002a: RUC20—The 20-km version of the Rapid Update Cycle. NWS Technical Procedures Bulletin 490, 30 pp. [FSL revised version available online at http://ruc.fsl.noaa.gov.]

——, D. Kim, and J. M. Brown, 2002b: Cloud/hydrometeor initialization in the 20-km RUC using GOES and radar data. Preprints, *10th Conf. on Aviation, Range, and Aerospace Meteorology,* Portland, OR, Amer. Meteor. Soc., 232–235.

——, G. A. Grell, J. M. Brown, T. G. Smirnova, and R. Bleck, 2004: Mesoscale weather prediction with the RUC hybrid isentropic–terrain-following coordinate model. *Mon. Wea. Rev.,* **132,** 473–494.

Bennett, A. F., 1992: *Inverse Methods in Physical Oceanography.* Cambridge University Press, 346 pp.

Black, T. L., 1994: The new NMC mesoscale Eta Model: Description and forecast examples. *Wea. Forecasting,* **9,** 265–278.

Bleck, R., and S. G. Benjamin, 1993: Regional weather prediction with a model combining terrain-following and isentropic coordinates. Part I: Model description. *Mon. Wea. Rev.,* **121,** 1770–1785.

Bratseth, A. M., 1986: Statistical interpolation by means of successive correction. *Tellus,* **38A,** 439–447.

Daley, R., 1991: *Atmospheric Data Analysis.* Cambridge University Press, 457 pp.

——, and E. Barker, 2001: NAVDAS: Formulation and diagnostics. *Mon. Wea. Rev.,* **129,** 869–883.

Davies, H. C., and R. E. Turner, 1977: Updating prediction models by dynamical relaxation: An examination of the technique. *Quart. J. Roy. Meteor. Soc.,* **103,** 225–245.

Dee, D. P., L. Rukhovets, R. Todling, A. M. Da Silva, and J. W. Larson, 2001: An adaptive buddy check for observation quality control. *Quart. J. Roy. Meteor. Soc.,* **127,** 2451–2471.

Derber, J. C., and A. Rosati, 1989: A global oceanic data assimilation system. *J. Phys. Oceanogr.,* **19,** 1333–1347.

Devenyi, D., and S. G. Benjamin, 2003: A variational assimilation technique in a hybrid isentropic-sigma coordinate. *Meteor. Atmos. Phys.,* **82,** 245–257.

Gustafsson, N., L. Berre, S. Hörnquist, X.-Y. Huang, M. Lindskog, B. Navascués, K. S. Mogensen, and S. Thorsteinsson, 2001: Three-dimensional variational data assimilation for a limited area model. Part I: General formulation and the background error constraint. *Tellus,* **53A,** 425–446.

Gutman, S. I., and S. G. Benjamin, 2001: The role of ground-based GPS meteorological observations in numerical weather prediction. *GPS Solutions,* **4** (4), 16–24.

Huang, X.-Y., and P. Lynch, 1993: Diabatic digital-filtering initialization: Application to the HIRLAM model. *Mon. Wea. Rev.,* **121,** 589–603.

——, K. S. Mogensen, and X. Yang, 2002: First-guess at the appropriate time: The HIRLAM implementation and experiments. *Proc. HIRLAM Workshop on Variational Data Assimilation and Remote Sensing,* Helsinki, Finland, Finnish Meteorological Institute, 28–43.

Ide, K., P. Courtier, M. Ghil, and A. C. Lorenc, 1997: Unified notation for data assimilation: Operational, sequential and variational. *J. Meteor. Soc. Japan,* **75,** 181–189.

Johnson, D. R., T. H. Zapotocny, F. M. Reames, B. J. Wolf, and R. B. Pierce, 1993: A comparison of simulated precipitation by hybrid isentropic-sigma and sigma models. *Mon. Wea. Rev.,* **121,** 2088–2114.

——, A. J. Lenzen, T. H. Zapotocny, and T. K. Schaack, 2000: Numerical uncertainties in the simulation of reversible isentropic processes and entropy conservation. *J. Climate,* **13,** 3860–3884.

Kim, D., and S. G. Benjamin, 2001: Cloud/hydrometeor initialization for the 20-km RUC using satellite and radar data. Preprints, *14th Conf. on Numerical Weather Prediction,* Fort Lauderdale, FL, Amer. Meteor. Soc., J113–J115.

——, ——, and J. M. Brown, 2002: Cloud/hydrometeor initialization in the 20-km RUC using radar and GOES data. Preprints, *15th Conf. on Numerical Weather Prediction,* San Antonio, TX, Amer. Meteor. Soc., 335–338.

Leidner, S. M., D. R. Stauffer, and N. L. Seaman, 2001: Improving short-term numerical weather prediction in the California coastal zone by dynamic initialization of the marine boundary layer. *Mon. Wea. Rev.,* **129,** 275–294.

Lorenc, A. C., 1981: A global three-dimensional multivariate statistical interpolation scheme. *Mon. Wea. Rev.,* **109,** 701–721.

——, R. S. Bell, and B. Macpherson, 1991: The Meteorological Office analysis correction data assimilation scheme. *Quart. J. Roy. Meteor. Soc.,* **117,** 59–89.

——, and Coauthors, 2000: The Met. Office global three-dimensional variational data assimilation scheme. *Quart. J. Roy. Meteor. Soc.,* **126,** 2991–3012.

Lynch, P., and X.-Y. Huang, 1992: Initialization of the HIRLAM model using a digital filter. *Mon. Wea. Rev.,* **120,** 1019–1034.

Macpherson, B., 1991: Dynamic initialization by repeated insertion of data. *Quart. J. Roy. Meteor. Soc.,* **117,** 965–991.

Miller, P. A., and S. G. Benjamin, 1992: A system for the hourly assimilation of surface observations in mountainous and flat terrain. *Mon. Wea. Rev.,* **120,** 2343–2359.

Moninger, W. R., R. D. Mamrosh, and P. M. Pauley, 2003: Automated meteorological reports from commercial aircraft. *Bull. Amer. Meteor. Soc.,* **84,** 203–216.

Parrish, D. F., and J. C. Derber, 1992: The National Meteorological Center's spectral statistical interpolation analysis system. *Mon. Wea. Rev.,* **120,** 1747–1763.

Purser, R. J., W.-S. Wu, D. F. Parrish, and N. M. Roberts, 2001: Numerical aspects of the application of recursive filters to variational statistical analysis with spatially inhomogeneous covariance. NOAA/NCEP Office Note 431, 34 pp.

Rabier, F., H. Järvinen, E. Klinker, J. F. Mahfouf, and A. Simmons, 2000: The ECMWF operational implementation of four-dimensional variational assimilation. I: Experimental results with simplified physics. *Quart. J. Roy. Meteor. Soc.,* **126,** 1143–1170.

Riishojgaard, L. P., 1998: A direct way of specifying flow-dependent background error correlations for meteorological analysis systems. *Tellus,* **50A,** 42–57.

Robinson, A. R., P. F. J. Lermusiaux, and N. Q. Sloan III, 1998: Data assimilation. *The Sea—Ideas and Observations on Progress in the Study of the Seas,* K. H. Brink and A. R. Robinson, Eds., The Global Coastal Ocean, Wiley, 541–594.

Rogers, E., D. Parrish, and G. DiMego, 1999: Changes to the NCEP operational Eta analysis. NOAA/NWS Technical Procedures Bulletin 454, 25 pp. [Available from National Weather Service, Office of Climate, Water, and Weather Services, 1325 East-West Highway, Silver Spring, MD 20910; also available online at http://www.nws.noaa.gov/om/tpbpr.shtml.]

Schreiner, A. J., T. J. Schmit, and W. P. Menzel, 2001: Clouds based on GOES sounder data. *J. Geophys. Res.,* **106** (D17), 20 349–20 363.

Schwartz, B. E., and S. G. Benjamin, 1995: A comparison of temperature and wind measurements from ACARS-equipped aircraft and rawinsondes. *Wea. Forecasting,* **10,** 528–544.

——, and ——, 2002: Verification of RUC surface forecasts at major U.S. airport hubs. Preprints, *10th Conf. on Aviation Meteorology,* Portland, OR, Amer. Meteor. Soc., 327–330.

Shapiro, M. A., 1981: Frontogenesis and geostrophically forced secondary circulations in the vicinity of jet stream–frontal zone systems. *J. Atmos. Sci.,* **38,** 954–973.

Skamarock, W. C., J. B. Klemp, and J. Dudhia, 2001: Prototypes for the WRF (Weather Research and Forecast) model. Preprints, *14th Conf. on Numerical Weather Prediction,* Fort Lauderdale, FL, Amer. Meteor. Soc., J11–J15.

Smirnova, T. G., J. M. Brown, and S. G. Benjamin, 1997: Evolution of soil moisture and temperature in the MAPS/RUC assimilation cycle. Preprints, *13th Conf. on Hydrology,* Long Beach, CA, Amer. Meteor. Soc., 172–175.

——, S. G. Benjamin, J. M. Brown, B. Schwartz, and D. Kim, 2000: Validation of long-term precipitation and evolved soil moisture and temperature fields in MAPS. Preprints, *15th Conf. on Hydrology,* Long Beach, CA, Amer. Meteor. Soc., 43–46.

Smith, T. L., S. G. Benjamin, B. E. Schwartz, and S. I. Gutman, 2000: Using GPS-IPW in a 4-D data assimilation system. *Earth Planets Space,* **52,** 921–926.

——, ——, S. I. Gutman, and B. E. Schwartz, 2003: Impact of GPS-IPW data on RUC forecasts. Preprints, *Seventh Symp. on IOS: The Water Cycle,* Long Beach, CA, Amer. Meteor. Soc., CD-ROM, 3.2.

Stauffer, D. R., and N. L. Seaman, 1990: Use of four-dimensional data assimilation in a limited-area mesoscale model. *Mon. Wea. Rev.,* **118,** 1250–1277.

——, and ——, 1994: Multiscale four-dimensional data assimilation. *J. Appl. Meteor.,* **33,** 416–434.

Wilson, J. W., N. A. Crook, C. K. Mueller, J. Sun, and M. Dixon, 1998: Nowcasting thunderstorms: A status report. *Bull. Amer. Meteor. Soc.,* **79,** 2079–2099.

Wolfe, D. E., and S. I. Gutman, 2000: Development of the NOAA/ERL ground-based GPS water vapor demonstration network: Design and initial results. *J. Atmos. Oceanic Technol.,* **17,** 426–440.